

COUPLING OF THERMAL AND ELECTRICAL PARAMETERS FOR  
SYSTEM-LEVEL POWER SYSTEM STUDIES

by

Mahbubur Rahman

A dissertation submitted to the faculty of  
The University of North Carolina at Charlotte  
in partial fulfillment of the requirements  
for the degree of Doctor of Philosophy in  
Electrical Engineering

Charlotte

2019

Approved by:

---

Dr. Valentina Cecchi

---

Dr. Badrul Chowdhury

---

Dr. Madhav Manjrekar

---

Dr. Maciej Noras

©2019  
Md Mahbubur Rahman  
ALL RIGHTS RESERVED

## ABSTRACT

MAHBUBUR RAHMAN. Coupling of thermal and electrical parameters for system-level power system studies. (Under the direction of Dr. Valentina Cecchi)

Conventional method of power system analysis uses predefined values of transmission line electrical parameters which are considered uniformly distributed along the overhead lines. Conductor temperatures of transmission lines are dependent on the time and space-varying nature of the external conditions, including weather which affects the line electrical parameters. A steady-state power system analysis method is developed in this thesis which is capable of integrating the dynamic line rating approach coupled with the non-uniform distribution of line electrical parameters. The proposed temperature-dependent power flow method provides a realistic representation of a power system network as well as offers a better estimate of system power handling capability with the development of temperature-dependent continuation power flow method (TD-CPF). Uncertainty in weather conditions data can also be coupled with the proposed method. The temperature-dependent steady-state analysis method is extended to incorporate the transient heat balance conditions of a system especially during change in system loads or branch contingencies. The proposed temperature-dependent power system analysis method was automated and its impacts on the large-scale system studies were investigated.

## ACKNOWLEDGEMENTS

I would like to acknowledge and thank my Ph.D. supervisor, Dr. Valentina Cecchi, for all her support and guidance in performing the research works for this dissertation. I thank Dr. Cecchi for being an amazing mentor throughout my doctoral studies, her continuous encouragement and motivation, and for sharing her passion of research with me. I want to thank Dr. Cecchi for giving me the opportunity to be a part of her research group in the Energy Production and Infrastructure Center (EPIC) at UNC Charlotte, of which I am extremely proud.

I would like to thank Dr. Badrul Chowdhury, Dr. Madhav Manjrekar, and Dr. Maciej Noras for serving on my doctoral dissertation committee, for continuously reviewing my work, and for sharing their valuable inputs and advices which helped me to improve the quality of this research. I would also like to thank Dr. Karen Miu from Drexel University for sharing her expertise with me and providing me with valuable suggestions.

I would like to express my gratitude to all the faculty members, fellow students and staff at the Energy Production and Infrastructure Center and Department of Electrical and Computer Engineering. I thank you for sharing your knowledge and interests with me. Thank you for all your help and friendship throughout the program.

Finally, I would like to thank my family, who has constantly supported me and kept unconditional faith in me.

Mahi

## TABLE OF CONTENTS

LIST OF TABLES	viii
LIST OF FIGURES	x
LIST OF ABBREVIATIONS	xii
CHAPTER 1 : INTRODUCTION	1
1.1 Overview	1
1.2 Background and Motivation	1
1.3 Conductor Temperature and System Level Analysis	3
1.4 Research Objectives	4
1.5 Research Contributions	5
1.6 Thesis Organization	7
CHAPTER 2 : REVIEW OF THE IMPACT OF WEATHER CONDITIONS ON POWER SYSTEMS	8
2.1 Overview	8
2.2 Weather Conditions and Conductor Temperature	8
2.3 Conductor Temperature and Line Electrical Parameters	9
2.4 Longitudinal Non-Uniformity of Electrical Parameters	10
2.5 Temperature-Dependent Line Modeling	10
2.5.1 Non-Uniformly Distributed Parameter Model	11
2.5.2 Multi-Segment Lumped Parameter Model	12
2.6 Impact on Steady-State System Analysis	14
CHAPTER 3 : TEMPERATURE-DEPENDENT POWER FLOW	16
3.1 Overview	16
3.2 Proposed TD-PF Method	16

3.2.1	TD-PF Algorithm	17
3.3	TD-PF with TD-LM	18
3.3.1	Algorithm	19
3.4	Simulation Results	21
3.4.1	4-Bus System	21
3.4.2	39-Bus System	25
CHAPTER 4 : TEMPERATURE-DEPENDENT TRANSMISSION CAPACITY ANALYSIS		28
4.1	Overview	28
4.2	TD-PF for Transfer Capacity	28
4.2.1	Algorithm	29
4.3	Case Study Considering Thermal and Voltage Stability Limit	31
4.4	Temperature-Dependent Continuation Power Flow	34
4.4.1	Algorithm	35
4.5	Simulation Results	39
CHAPTER 5 : IMPACT OF DATA UNCERTAINTY ON TEMPERATURE-DEPENDENT POWER SYSTEM ANALYSIS		46
5.1	Overview	46
5.2	Affine Arithmetic (AA) for Data Uncertainty	46
5.2.1	AA-based Heat Balance Equation	48
5.2.2	Impact of Uncertainties on Line Parameters and Conductor Temperatures	49
5.3	AA-based Temperature-Dependent Power Flow	52
5.4	Simulation Results	54
CHAPTER 6 : TEMPERATURE-DEPENDENT POWER FLOW COUPLED WITH NON-STATIC HEAT BALANCE		63

6.1	Overview	63
6.2	Non-Steady-State Heat Balance Equation	64
6.3	Time-Dependent and Temperature-Dependent Power System Simulation	64
6.3.1	Algorithm for the proposed method	66
6.4	Simulation Results	69
6.4.1	2-Bus System	69
6.4.2	14-Bus System	77
CHAPTER 7 : CONCLUSION AND FUTURE WORK		80
7.1	Overview	80
7.2	Summary of Contributions	81
7.3	Future Work	84
REFERENCES		86
APPENDICES		96
Appendix A: Line Model Segmentation and		97
Appendix B: Generic Codes		101
VITA		104

## LIST OF TABLES

TABLE 3.1: Line Model Segmentation for 4 Bus Network	23
TABLE 3.2: Conductor Temperatures ( $T_c$ ) for 4 Bus Network from TD-PF	24
TABLE 3.3: Branch Losses for 4 Bus Network	24
TABLE 3.4: Measured Wind Speeds and Ambient Temperatures for 39-Bus System	26
TABLE 3.5: Comparison of Conductor Temperatures for 39 Bus Network	27
TABLE 4.1: Comparison of $\lambda_{max}$ (4-bus system)	32
TABLE 4.2: Line Currents to Reach Thermal and Voltage Stability Limits	33
TABLE 4.3: Comparison of $\lambda_{max}^{eff}$ for 4-Bus System	34
TABLE 4.4: Comparison of $\lambda_{max}$ and $T_c$ at $\lambda_{max}$ for Cases 1-4	45
TABLE 5.1: Weather Data for summer and winter at 12 Noon	51
TABLE 5.2: Ambient temperatures and wind speeds	54
TABLE 5.3: TD-PF results for 4-bus system	56
TABLE 5.4: TD-PF results for 4-bus system	57
TABLE 5.5: TD-PF results for 4-bus system	58
TABLE 5.6: Comparison of Branch Currents	59
TABLE 5.7: Weather data for 4-bus system	60
TABLE 5.8: TD-PF results for 4-bus system	62
TABLE 6.1: Loading conditions for the 2-bus system	69
TABLE 6.2: Pre-contingency results from TD-PF – Case A	70
TABLE 6.3: Resulting limiting factor and critical time – Case A	72
TABLE 6.4: Pre-contingency results from TD-PF – Case B	72
TABLE 6.5: Resulting limiting factor and critical time – Case B	74

TABLE 6.6: Pre-contingency results from TD-PF – Case C	75
TABLE 6.7: Resulting limiting factor and critical time – Case C	77
TABLE 6.8: Comparison of time required to reach limiting factor or new steady-state condition	78

## LIST OF FIGURES

FIGURE 2.1: Differential Approach to Spatial Non-Uniformity of Line Parameters	12
FIGURE 2.2: Multi-segment line models	13
FIGURE 3.1: Proposed Temperature-Dependent Power Flow	18
FIGURE 3.2: Line Model Segmentation Outputs	19
FIGURE 3.3: Integration of T-D line modeling with temperature-dependent PF	20
FIGURE 3.4: 4-Bus System	22
FIGURE 3.5: 39-Bus System	25
FIGURE 4.1: Power handling capability studies using temperature-dependent power flow	30
FIGURE 4.2: P-V plots for bus 2 for each case of the 4-bus system	31
FIGURE 4.3: P-V plots with thermal limits	34
FIGURE 4.5: Temperature-Dependent Continuation Power Flow	37
FIGURE 4.6: $T_c$ profile and line model segmentation for case 2	40
FIGURE 4.7: Conventional CPF and TD-CPF plots for the single-segment line model at weighted average conductor temperature (Cases 1 and 3)	42
FIGURE 4.8: Conventional CPF and TD-CPF plots for the 3-segment line model (Cases 2 and 4)	43
FIGURE 5.1: Conductor temperature as a function of ambient temperature and wind speed during the summer season	52
FIGURE 5.2: Proposed Temperature-Dependent Power Flow with Data Uncertainty	53
FIGURE 5.3: 4-bus system	54
FIGURE 5.4: PV plot different summer and winter	58
FIGURE 5.5: Two-area 30-bus system	60
FIGURE 5.6: Boundary of voltage magnitudes	61

FIGURE 5.7: Conductor temperatures from proposed TD-PF	61
FIGURE 5.8: PV plot for 30-bus system	62
FIGURE 6.1: Temperature-dependent contingency analysis	68
FIGURE 6.2 : A 2-line 2-bus system	69
FIGURE 6.3: Line 1 conductor temperature – Case A	71
FIGURE 6.4: Line 1 current – Case A	71
FIGURE 6.5: Line 1 real power loss – Case A	72
FIGURE 6.6: Line 1 current – Case B	73
FIGURE 6.7: Line 1 conductor temperature – Case B	74
FIGURE 6.8: Line 1 real power loss – Case B	74
FIGURE 6.9: Line 1 current – Case C	75
FIGURE 6.10: Line 1 conductor temperature – Case C	76
FIGURE 6.11: Branch 1 conductor temperature – Case C	77

## LIST OF ABBREVIATIONS

$T_a$	Ambient Temperature ( $^{\circ}\text{C}$ )
$v_w$	Wind speed (m/s)
$T_c$	Conductor Temperature ( $^{\circ}\text{C}$ )
$T_c^{max}$	Maximum allowable conductor Temperature ( $^{\circ}\text{C}$ )
$N_{Re}$	Reynold Number
$Q_c$	Convection heat loss ( $\text{W}/\text{m}^2$ )
$Q_s$	Solar heat gain ( $\text{W}/\text{m}^2$ )
$Q_r$	Radiated heat loss ( $\text{W}/\text{m}^2$ )
$k_f$	Thermal conductivity of air temperature $\text{W}/(\text{m}\cdot^{\circ}\text{C})$
$K_{angle}$	Wind direction factor (-)
$H_e$	Elevation of conductor above sea level (m)
$\alpha$	Solar absorptivity (-)
$\varepsilon$	Emissivity (-)
$l$	Line length (miles)
$r$	Resistance (Ohm)
$X_L$	Line inductive reactance (Ohm)
$X_C$	Line capacitive reactance (Ohm)
$I$	Line current (Amps)
$f$	Frequency (Hz)
$Z$	line impedance (Ohm)
$\lambda_{max}$	Maximum loading parameter (from continuation power flow)
$\lambda$	Loading parameter (in continuation power flow)

$\lambda_{max}^{eff}$	Maximum effective loading parameter (from continuation power flow)
$\Delta T_c$	Conductor temperature increment (°C)
$\Delta t$	Time-step increase during conductor temperature increment (minutes)
$T_c^{diff}$	Difference in conductor temperature within a transmission line (°C)
$P_i$	Real power flow from sending end bus (MW)
$P_j$	Real power flow into receiving end bus (MW)
$Q_i$	Reactive power flow from sending end bus (Mvar)
$Q_j$	Reactive power flow into receiving end bus (Mvar)
$P_{loss(i-j)}$	Real power loss in line i-j (MW)
$Q_{loss(i-j)}$	Reactive power loss in line i-j (Mvar)
$G_{ij}$	Real part of the $ij^{th}$ element of admittance matrix
$B_{ij}$	Imaginary part of $ij^{th}$ element of admittance matrix
$\delta$	Voltage angle difference (rad), $\delta_{ij} = \delta_i - \delta_j$
$\delta_i$	Voltage angle at the sending end (rad)
$\delta_j$	Voltage angle at the receiving end (rad)
$g$	Conductance (S)
$d$	Conductor diameter (m)
$d_{eq}$	Equivalent distance between conductors (m)
$\zeta$	Noise variable for uncertain parameters (-)

## CHAPTER 1: INTRODUCTION

### 1.1 Overview

The focus of this thesis lies on the system-level impact of the weather conditions on power transmission networks, in order to maximize the utilization of the existing transmission lines. The time and space-varying nature of weather conditions [1], [2] is exploited in this work to obtain a better estimation of the current-carrying capacity of the overhead lines. The dynamic thermal rating approach [1]-[3] is coupled with a temperature dependent line modeling method [4]-[6] to account for the longitudinal variation of weather conditions. A temperature-dependent power flow method incorporating the dynamic line rating and temperature-dependent line modeling has been introduced in this work to study the impact of weather conditions on power system analysis. The proposed power flow method incorporating weather conditions is utilized to determine the thermal and voltage stability limit of a system during steady-state conditions as well as during transient thermal conditions.

The following topics are presented in this chapter:

- Background and motivation for the work;
- Research objectives and contributions;
- Overview of the organization of the thesis.

### 1.2 Background and Motivation

With the increase in electric power generation and the emphasis on the integration of renewable energy sources, many of the transmission lines are operating close to or

beyond their nominal ratings [7]-[10]. Increasing the transmission capacity of the power grids is, therefore, of utmost importance for reliable and affordable delivery of electric power, as well as for maximum integration of the renewable energy sources. While construction of new transmission links is an option to increase the system capacity, building new lines can be cost-prohibitive, time consuming, and most importantly, constrained by the lack of availability of land corridors [11]-[13].

As system reinforcements are considered, it is also necessary to re-evaluate historical approaches used to set transmission line capabilities. Traditionally, predefined weather conditions are used to calculate thermal limits of transmission lines, known as static line ratings [14]-[17]. As a conservative set of weather parameters are used in this static line rating approach [14], [18] the line ampacity calculated using this method is often not very realistic. With the proliferation of weather measurements and the increase in availabilities of power component sensors and measurements [19]-[22], dynamic line rating approach has been proposed, which uses measured values of weather conditions to obtain line thermal rating. According to studies, dynamic thermal rating has the potential to enhance the line ampacity by as high as 53% compared to the static thermal rating approach [23]. However, the dynamic thermal rating does not consider the longitudinal variation of the weather conditions. As transmission lines pass through different geographic locations, it can experience different weather conditions along the lengths. In order to account for the longitudinal variation of weather conditions and conductor temperatures and the resultant non-uniformity of line impedance, temperature-dependent line modeling approaches have been developed [4], [6], [24]-[25]. This consideration of non-uniform line impedance affects the maximum power transfer capability of a

transmission system considering both thermal and voltage stability limits [4], [25]. System-level analysis of the impacts of the time and space-varying nature of the weather conditions are required to obtain a better representation of a power system network; also for an improved estimation of the maximum power handling capability of a transmission network, which is the primary focus of this research.

Traditional power system analysis methods, i.e. power flow and state estimation, do not consider any external conditions, including weather conditions, aging of the lines and environmental pollutions [26]-[27]. Preset values of line electrical parameters, calculated at assumed conductor temperatures, are used in traditional power system analysis methods. As weather parameters and resultant conductor temperatures are not taken into account in the traditional methods, they are also unable to provide information about branch thermal conditions in a system [28]. In order to perform the system-level analysis of the impact of the variation in ambient conditions, weather parameters need to be incorporated into state estimation and power flow analysis. An integrated approach to power system analysis needs to be developed to take into account the available weather conditions as well as possible longitudinal variations in conductor temperatures.

### 1.3 Conductor Temperature and System Level Analysis

Conventionally Newton-Raphson power flow methods use a predefined set of line parameter values to perform the conventional power flow analysis. The values of line electrical parameters used in these methods are usually taken from conductor manuals and reference books, which are based on assumed weather conditions and branch loading [27], [29]. State estimation method incorporating the conductor temperatures was proposed in [30], where a simplified assumption for the impact of ambient temperature on conductor

temperature was considered. A temperature-dependent power flow method capable of incorporating weather conditions was developed in [31]. However, linearized versions of the heat equations from [32] were used for that method, which may introduce inaccuracy in the study of impact of weather conditions on the power flow results.

Impact of conductor temperature on both thermal and system voltage stability limits was studied in few of the research studies [33], [34]. These studies analyzed the impact of conductor temperatures for congestion management and optimal power flow solutions. However, most of the works consider the conductor temperatures only for thermal limits and not for the voltage stability limit. A study incorporating the heat balance equation and voltage collapse point was performed in [35], but it did not account for the spatial variation in conductor temperatures.

#### 1.4 Research Objectives

The objectives of this thesis work can be presented as follows:

- Revisiting the impact of weather conditions on the modeling of transmission lines:
  - Calculation of conductor temperatures using heat balance equation from IEEE Std. 738
  - Variation of conductor temperatures along the length of a line,
  - Temperature-dependent line modeling approaches
    - Differential approach
    - Segmented approach

- Investigation:
  - Impact of the non-uniformity of line parameters on steady-state analysis of power systems
  - Impact of varying weather conditions on the power handling capabilities of the a transmission network and of individual lines in the network considering thermal and voltage stability limits;
  - Impact of weather uncertainties on the limiting factors to maximum power transfer.
- Development:
  - A power flow algorithm which is capable of integrating the time and space-varying weather conditions into account for steady-state analysis;
  - A toolbox which can determine the maximum power transfer limit of a system during both steady-state and non-static thermal conditions.

### 1.5 Research Contributions

The contribution of this thesis can be summarized as follows:

- Coupling of thermal and electrical parameters of transmission lines:
  - To study the system-level impact of weather conditions on power system analysis;
  - To obtain a more accurate estimation about the loading capabilities of different transmission lines in a system.
- Development and implementation of a Temperature-Dependent Power Flow (TD-PF), which is capable of:

- Accounting for the variation in weather parameters into power flow analysis;
- Providing a more realistic representation of a system compared to the conventional methods;
- Delivering conductor temperatures of the transmission lines in a system along with the electrical parameters;
- Development of a Temperature-Dependent Continuation Power Flow (TD-CPF) which can be used to:
  - Find a better estimation of the system maximum power handling capability;
  - Determine the primary power limiting factor comparing thermal limit and voltage stability limit;
- Introduction of an Affine Arithmetic based system analysis approach to account for the uncertainty in weather conditions:
  - The temperature-dependent power flow based on affine arithmetic can be used when there is uncertainties in the external conditions datasets.
  - Rather than providing a single floating point number as a solution, this approach provides a non-deterministic solution to the problem.
- A power flow approach accounting for transient thermal conditions of overhead lines:
  - Proposed method can determine the maximum power transfer limit of a transmission network during a variation in load or outages in one or branches;

- The time required to reach the transfer limit during the non-static thermal condition can be obtained using this approach.

## 1.6 Thesis Organization

The thesis is structured as follows:

- In Chapter 2, literature reviews on the impact of weather conditions on the line electrical parameters and line thermal rating are discussed, including the temperature-dependent line modeling approaches.
- In Chapter 3, a power flow method capable of incorporating the variation in weather conditions into power system analysis is introduced.
- In Chapter 4, Temperature-Dependent Continuation Power Flow (TD-CPF) method is described, which can account for the change in conductor temperature at each step increase in the loading parameter.
- In Chapter 5, a method to integrate the uncertainties in weather conditions into the proposed power flow method is discussed and the impact of the mentioned uncertainties on the system power handling capabilities is investigated.
- In Chapter 6, the impact of transient thermal conditions on power system is analyzed; and the variation in the thermal and voltage stability limits during the non-static heat balance is investigated.
- Finally in Chapter 7, the accomplishments and contributions of this research work are summarized and the future work and vision are presented.

## CHAPTER 2: REVIEW OF THE IMPACT OF WEATHER CONDITIONS ON POWER SYSTEMS

### 2.1 Overview

Electric power lines (transmission and distribution) are integral component of the power system. System operators generally limit the transport capability of electric power lines using a static thermal rating, which is clashing with the constant increase in demand of electric power, in conjunction with the strong push for integration of renewable sources of energy to the existing network.

This chapter provides a review of the temperature-dependent line modeling including:

- Relationship between weather conditions and conductor temperatures,
- Impact of conductor temperatures on line electrical parameters, and
- Line modeling based on longitudinal variation in conductor temperatures

### 2.2 Weather Conditions and Conductor Temperature

External conditions including weather conditions such as wind speed, wind direction, ambient temperature, air pressure etc. can impact the thermal rating of a transmission line. Stead-state heat balance equation from IEEE Std. 738 demonstrates the effects of different ambient conditions on line ampacity [32]. For a set maximum allowable

conductor temperature and known or assumed values of weather parameters, the maximum allowable line current can be obtained using (1).

$$Q_c + Q_r = Q_s + I^2 R(T_c^{\max}) \quad (2.1)$$

The heat balance equation can be modified in such a way that it can provide the conductor temperature of a transmission line for known value of line current and weather parameters. A conservative and fixed set of weather parameters, i.e. low wind speed and high ambient temperature, are used in this equation to calculate the conductor temperature during the static line rating approach, while dynamic line rating approaches use measured data from weather stations or installed sensors as inputs for the heat balance equation [22], [36]-[38].

### 2.3 Conductor Temperature and Line Electrical Parameters

A transmission line model consists of four electrical parameters [27], [39]:

- r: series resistance per unit length
- l: series inductance per unit length
- g: shunt conductance per unit length
- c: shunt capacitance per unit length

Among the above mentioned four electrical parameters line series resistance is directly affected by the conductor temperatures. Using the linear relationship between temperature and resistance, as shown in (2), the line series resistance can be obtained for a specific conductor temperature [40].

$$R(T_c) = R_{ref} [1 + \alpha(T_c - T_{ref})] \quad (2.2)$$

As the line series impedance is composed of line resistance and inductive reactance, it also gets impacted by the conductor temperature as [27] –

$$Z(T_c) = R(T_c) + jX_L \quad (2.3)$$

#### 2.4 Longitudinal Non-Uniformity of Electrical Parameters

Transmission line models that are currently used in power systems cannot take the longitudinal variation in conductor temperature into account. As long transmission lines pass through various geographic locations and different weather conditions, the assumption of constant conductor temperature and uniformly distributed impedance throughout the line may not be realistic [4], [44]. Therefore, the line impedance is a function of position along the line, i.e. non-uniformly distributed, as follows (3):

$$Z(T_c(x)) = R(T_c(x)) + jX_L \quad (2.4)$$

Where

$T_c(x)$	$T_c$ as a function of position along the line, $x$
$Z(T_c(x))$	impedance as function of $T_c(x)$
$R(T_c(x))$	resistance dependent on $T_c(x)$
$X_L$	inductive reactance, independent of $T_c(x)$

#### 2.5 Temperature-Dependent Line Modeling

In order to consider this non-uniformity in line conductor temperatures, and therefore in line impedance, different approaches have been proposed in previous studies, though many of those studies are regarding the impact of non-uniformity of line electrical parameters for electromagnetic transient [45], [46]. According to the steady-state analysis

on non-uniformity of line electrical parameters there are two primary methods of line modeling conforming to the longitudinal variation in conductor temperature [41], [47].

### 2.5.1 Non-Uniformly Distributed Parameter Model

This modeling approach considers shunt admittance  $y$  and line impedance  $z(x)$  to be distributed along the transmission line [47]-[49]. A usual assumption is to neglect shunt conductance as it is very small. Thus, shunt admittance  $y$  is represented by

$$y = \frac{j}{x_c} \quad (2.5)$$

Line series impedance  $z(x)$  is determined by (3).

The quantities of resistance  $r(x)$ , inductive reactance  $xL$  and capacitive reactance  $x_c$  are given in per unit length.  $j$  denotes the imaginary part. The assumption on  $r(x)$  is that it can be represented by a power series (4) as follows:

$$yz(x) = \sum_{k=0}^{\infty} b_k x^k \quad (2.6)$$

The solution of these equations yields the course of voltage and current along the transmission line and also consists of a power series, given by equations (5) and (6) below.

$$V(x) = \frac{1}{y} \sum_{n=1}^{\infty} a_n x^{n-1}$$

$$a_{n+2} = \frac{\sum_{l=0}^n a_l b^{n-l}}{(n+2)(n+1)} \quad (2.7)$$

Where  $b_n$  are the coefficients of the power series representing line impedance (4). Since the solution is an infinite series, practically, it is cut off at some order. This introduces an error which needs to be estimated.

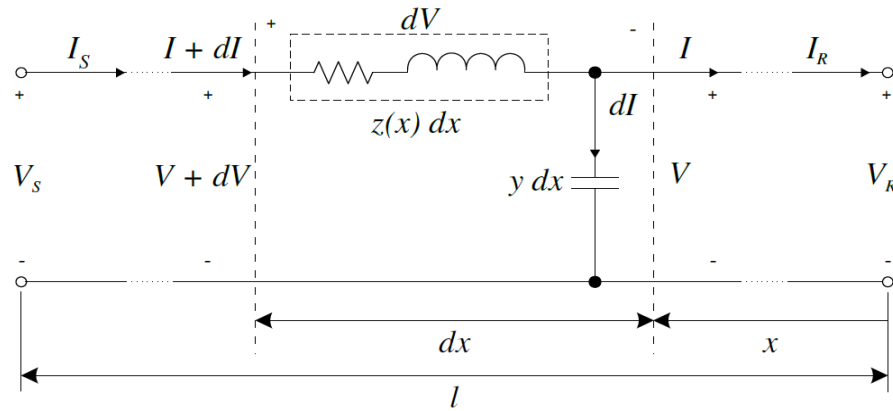


Figure 2.1: Differential Approach to Spatial Non-Uniformity of Line Parameters

### 2.5.2 Multi-Segment Lumped Parameter Model

A line modeling approach was used to divide the line model into multiple lumped segments, where each segment impedance is representative of the conductor temperature that that specific line section is subjected to. The number of segments of the line model depends on the degree of longitudinal change in conductor temperature, and the length of the transmission line. In order to appropriately segment the line model, a threshold value in terms of conductor temperature difference between any two points along the line would be introduced [41], [54]. Whenever the difference in conductor temperature between two points along the line reaches the threshold value,  $\Delta T_c^{th}$ , a segment is created. Each of the segments has its own weighted average conductor temperature, from which line impedance for each segment can be calculated as is depicted in Figure 2.2.

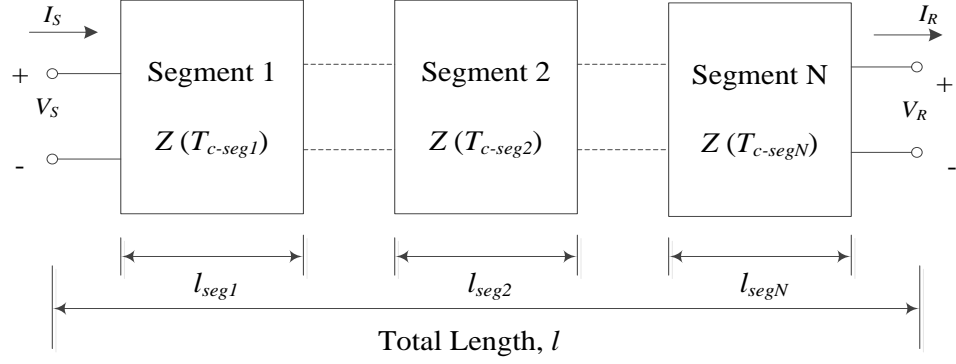


Figure 2.2: Multi-segment line models

Figure 2.2 shows an example line model with multiple lumped segments. The difference in conductor temperature between the beginning of segment 1, and the beginning of segment 2 is less than or equal to  $\Delta T_c^{th}$ , and so on. The conductor temperature for a single segment is calculated using a weighted average. Given  $t_1, t_2, \dots, t_n$  are conductor temperatures at points within a segment length, and  $t_{th}$  is the end-point temperature of the segment, the weighted average of that segment conductor temperature can be calculated as follows:

$$T_{seg} = \frac{\left(\frac{t_i + t_{i+1}}{2}\right)s_1 + \left(\frac{t_{i+1} + t_{i+2}}{2}\right)s_2 + \dots + \left(\frac{t_{n-1} + t_n}{2}\right)s_n + \left(\frac{t_n + t_{th}}{2}\right)s_{th}}{s_1 + s_2 + \dots + s_n + s_{th}} \quad (2.8)$$

where  $s_1, \dots, s_n$  are the distances between consecutive measuring points, and  $s_{th}$  denotes the distance between the last measuring unit and the point where the segment ends (if the segment end point is not a measuring point, its conductor temperature can be extrapolated).

## 2.6 Impact on Steady-State System Analysis

The variation in the weather conditions can impact the steady-state analysis of power system. Conventionally used power system analysis methods does not account for the weather conditions and conductor temperatures [50]-[51]. Instead of using measured values of weather conditions corresponding line electrical parameters, conventional methods use preset line parameters which may not represent the realistic conditions of a power system network [52]. Without obtaining a realistic representation of a network, it would also be difficult to determine the accurate power handling capability of a system [53].

There have been researches performed to integrate the weather conditions into system level power system analysis. [30], [31] incorporated the variation in conductor temperatures into power flow analysis and state-estimation analysis. These approaches use a very simplified version of the heat balance equation [32], and therefore fails to accommodate some of the external parameters into the temperature-dependent analysis of power system. However, as these approaches considers the conductor temperature for steady-state analysis, they are capable of providing information about thermal conditions of the branches in a system along with the electrical parameters.

Integration of the weather conditions and resultant conductor temperatures makes it possible to determine the power handling capability of a system in terms of both thermal and voltage stability limits. Studies in [34], [54] conspired both of the limiting factors for the determination of transfer limit of a system. [33] studied both thermal and voltage stability limits to determine the optimal operational region of a power system. However

these methods did not show the incorporation of the heat balance equation as well as the impact of all the weather conditions on the system.

Weather conditions can also impact the power transfer capability of a system during a non-static thermal condition, esp. during the outage of branch in the system or an increase in the system load. Research performed in this area considers only the change in thermal limit during a non-static thermal condition [55]-[56], does not study its impact on the voltage stability limit under these conditions. The varying line electrical parameters during the non-static thermal conditions are also not considered in the studied performed so far [57].

An integrated toolbox is proposed in this thesis to incorporate the external conditions into the steady-state system analysis and its impact on the primary limiting factors to maximum power transfer of a power system network. The proposed methodology can also be extended to study the impact of non-static thermal conditions on the power handling capabilities of the system as well as to investigate the impacts of the data uncertainties on the system-level analysis.

## CHAPTER 3: TEMPERATURE-DEPENDENT POWER FLOW

### 3.1 Overview

A temperature-dependent power flow method which is capable of integrating the weather conditions and resulting conductor temperatures into steady-state analysis of power system is proposed in this chapter. The proposed approach is capable of providing thermal conditions of the branches of the system alongside the electrical parameters. This chapter has two major sections:

- Development of a power flow method incorporating the weather conditions, and
- Integrating the temperature-dependent line modeling approaches into the proposed power flow method.

### 3.2 Proposed TD-PF Method

Conventionally Newton-Raphson power flow methods use a predefined set of line parameter values to perform the analysis of power systems. Therefore, the traditional load flow studies can generate a substantial margin of error when compared to real-time measurements [31], [58]. There have been few approaches developed to consider the weather conditions into power system state estimation, and power flow studies. Researchers in [31], incorporated the heat balance equation into the conventional power flow algorithm, whereas [30] integrated the conductor temperatures into power system

state estimation analysis. However, linear approximation of the heat balance equation was used in these studies which can introduce deviation from the actual thermal conditions of the line conductors. In this work, the solution of the conductor temperature from the non-linearized heat balance equation, and the solution of the power flow equations are determined sequentially within each iteration of the proposed method. The proposed power flow method provides the following outputs:

- i) Steady-state conductor temperature of each line in the system,
- ii) Voltage magnitude and phase at each bus, as in traditional power flow.

### 3.2.1 TD-PF Algorithm

An initial guess of the conductor temperature ( $T_c$ ) is made. For that  $T_c$ , line resistances are determined and an initial power flow is performed. The line current(s) are then calculated and fed into the heat balance equation (1), together with the weather parameters (which can be measured, given, or predicted), to obtain the updated  $T_c$ . It is noted that the heat balance equation is highly nonlinear [14], [15]. A Newton code-based solution method to solve non-linear equations [59] was used in this work to determine line conductor temperatures from the heat balance equation. In the power flow equations (4), it can be seen that all the elements of the Y matrix are functions of conductor temperatures ( $T_c$ ) of the respective iteration steps, and the  $T_c$  are functions of the locations along the line,  $x$ . Therefore, the values of  $T_c$  is used to update the line resistance at each iteration. The process continues until the difference in  $T_c$  for two subsequent iterations falls within a predefined tolerance, and the value of steady-state conductor temperature,  $T_c^{ss}$ , is determined. Fig. 3.1 shows the procedure of the proposed temperature-dependent power flow algorithm with a flowchart.

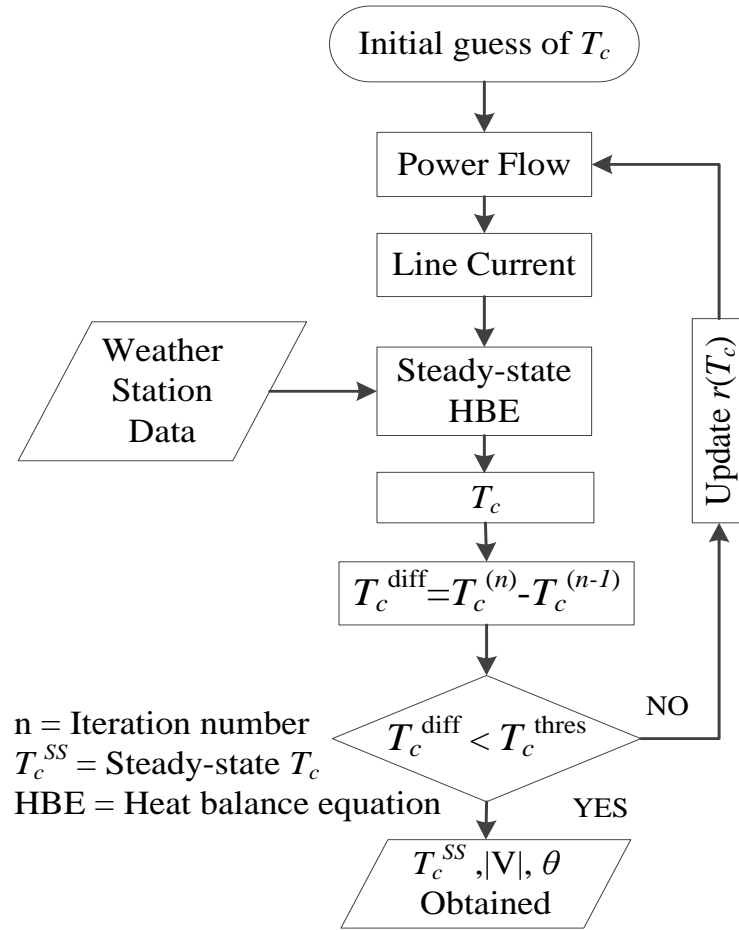


Figure 3.1: Proposed Temperature-Dependent Power Flow

### 3.3 TD-PF with TD-LM

The above described approach of temperature-dependent power flow considers ambient conditions and obtains conductor temperature, assumed constant along each line. However, temperature-dependent line modeling is needed to account for effects of longitudinal variations in ambient conditions (and consequently in conductor temperature and line parameters). The next subsection details how the TD-PF algorithm can incorporate these temperature-dependent line models.

In order to incorporate the variation of weather conditions along the line into the proposed temperature-dependent power flow, the previously described line model segmentation approach is used. Using the weather data and calculating line currents from an initial power flow, a conductor temperature ( $T_c$ ) profile is created for each line using the steady-state heat balance equation [41], [47], [54]. If available, measurement from conductor temperature sensors can be used directly. Once a  $T_c$  profile is defined for each line, the temperature-dependent line model segmentation is performed. Each line model is divided into multiple lumped parameter segments depending on the threshold value of the difference of conductor temperature ( $T_c^{thres}$ ) along the line [54].

The temperature-dependent line modeling approach and its outputs are presented briefly in Fig. 3.2.

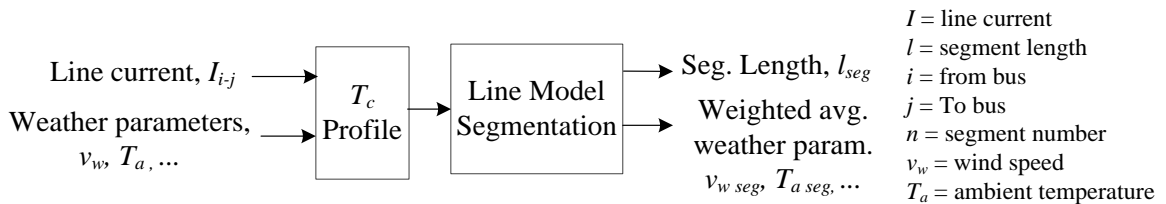


Figure 3.2: Line Model Segmentation Outputs

### 3.3.1 Algorithm

Segment lengths,  $l_{seg}$ , and weighted average weather parameters ( $v_w seg, T_a seg$ ) for each segment are calculated from line model segmentation. The weighted average weather parameters are required to update the conductor temperatures in the iterative process of the temperature-dependent power flow method. Once the line models are divided into multiple segments, the transmission system model is updated accordingly. The start/end of a segment within a line model is considered a load-less PQ bus. The introduction of these

load-less PQ buses effectively increases the size of the Y-bus matrix, which can impact computational time. However, this increased number of buses would also increase the sparsity of the matrix which can be exploited using, for example, the techniques described in [60], or Kron's reduction [61] can be employed.

The proposed power flow approach is performed on the updated network model. Fig. 3.3 graphically summarizes the procedure of taking the longitudinal variations in weather conditions into account via temperature-dependent line models, and incorporating it with the temperature-dependent power flow shown in the previous subsection.

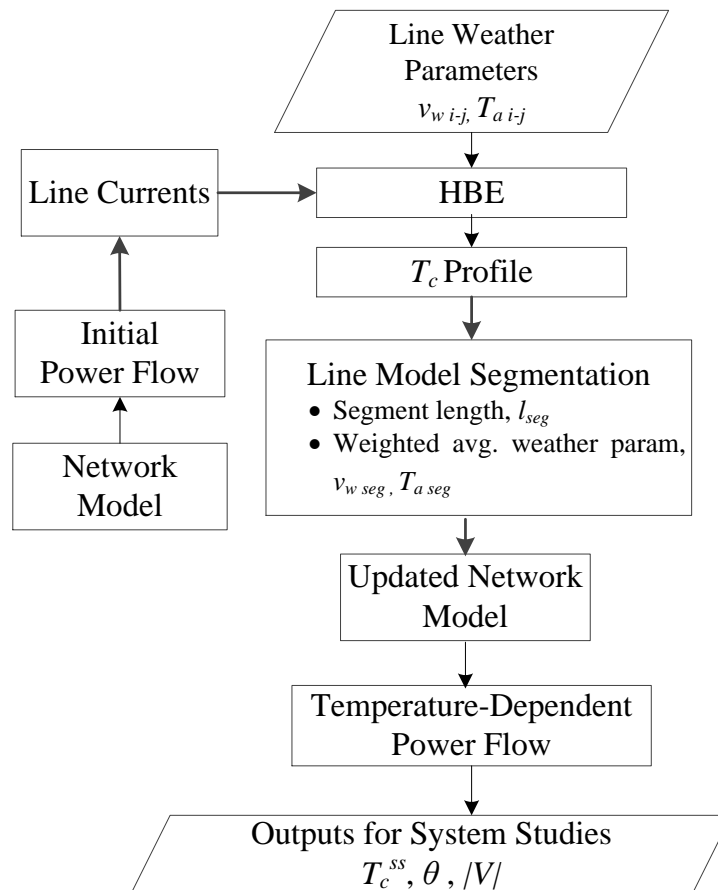


Figure 3.3: Integration of T-D line modeling with temperature-dependent PF

### 3.4 Simulation Results

The proposed power flow method is performed on two different sizes of power transmission networks- one smaller (4-bus system) and the other of larger scale (39-bus system). The impact of taking the weather conditions into power flow analysis is studied for both of the cases and the results are compared to conventional power flow method.

#### 3.4.1 4-Bus System

A 4-bus transmission network is used for the case study. The network is composed of five transmission lines of different lengths and all the lines are made of ACSR Rook conductor. The electrical parameters for the Rook conductor can be found in [29]. Each of the branches is considered to have multiple weather stations along its length as presented in Fig. 3.4. For this work, realistic weather data was mimicked using regional weather station data from the Charlotte-Douglas International Airport in North Carolina [62]. Three different cases will be studied for the 4-bus system – conventional power flow with  $\pi$ -line models, the proposed TD-PF approach with  $\pi$ -line models, and the TD-PF with the temperature-dependent line modeling.

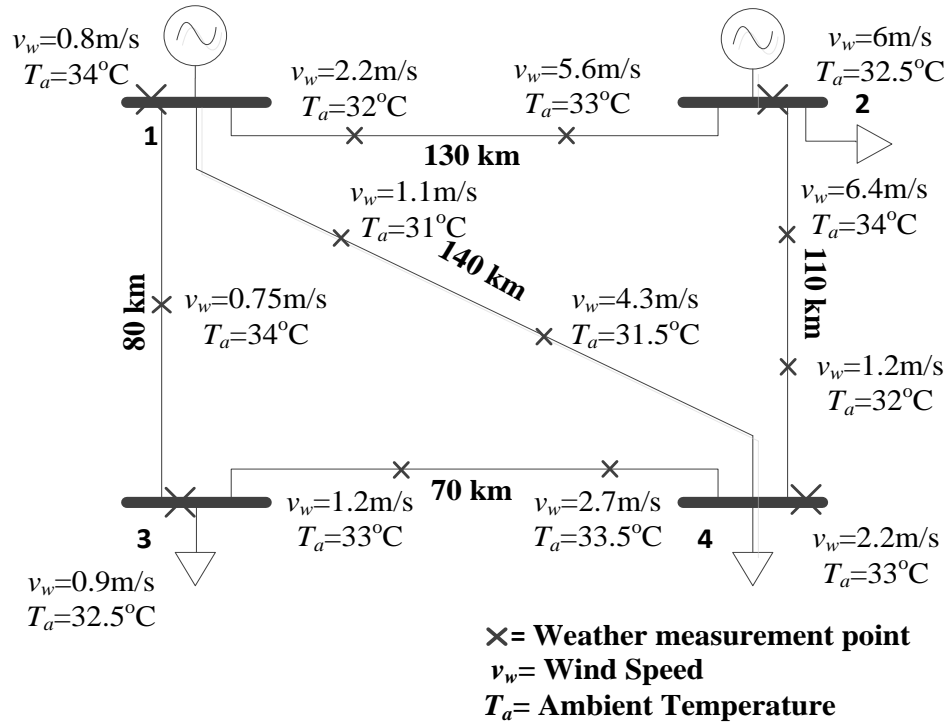


Figure 3.4: 4-Bus System

*Case A:* Conventional power flow method is used in this case, which does not take the measured weather conditions into account. Commonly used predefined weather conditions are considered in this case to calculate the conductor temperatures [63]. Specifically, an ambient temperature of  $40^\circ\text{C}$  and a wind speed of  $0.6 \text{ m/s}$  are used [40].

*Case B:* The proposed temperature-dependent power flow for steady-state analysis is used but the longitudinal variation of weather conditions is not considered. The measured weather conditions along a line which account for the lowest line ampacity (or highest  $T_c$ ) are used.

*Case C:* The temperature-dependent power flow approach is now coupled with temperature-dependent line modeling (TD-LM). Using a threshold value of  $5^\circ\text{C}$  for the conductor temperature difference between two points, line model segmentation is applied. The lengths of each segment, the corresponding weighted average wind speed and the

ambient temperature for each segment (resulting from the line model segmentation as discussed in Section 3.2) are presented in Table 3.1.

Table 3.1: Line Model Segmentation for 4 Bus Network

Branch #	From Bus	To Bus	Length (km)	# of Segs	Seg Length, $l_{seg}$ (km)	Seg. $v_w$ (m/s)	Seg. $T_a$ ( $^{\circ}$ C)
1	1	2	130	3	27	1.24	33.2
					34	2.40	32.66
					69	5.3	32.75
2	1	3	80	1	80	0.86	33.63
3	1	4	140	2	75	1.38	32.25
					65	3.37	32.75
4	2	4	110	3	50	6	33.1
					15	3.35	32.7
					45	1.7	32.35
5	3	4	70	1	46	1.5	33
					24	2.45	33.25

Table 3.2 denotes resulting conductor temperatures,  $T_c$ . Values for case B are lower than those of Case A, which is expected as even the lowest measured wind speed ( $v_w$ ) for each line is still higher than the value of  $v_w$  used in static line rating, and the highest measured ambient temperature ( $T_a$ ) for each line is lower than  $40^{\circ}$ C. Case C takes the variation of the measured weather parameters into account. Therefore, the respective line  $T_c$  for case C are lower than the  $T_c$  from Case A and Case B.

Table 3.2: Conductor Temperatures ( $T_c$ ) for 4 Bus Network from TD-PF

Branch #	Conventional PF Case A ( $^{\circ}\text{C}$ )	Proposed TD-PF Case B ( $^{\circ}\text{C}$ )	Proposed TD-PF with TD-LM Case C (MW)
1	67	59.9	53.0
			48.0
			43.2
2	62	54.8	50.7
3	56	48.2	42.8
			39.2
4	66	55.5	41.9
			44.8
			49.1
5	59	48.8	44.6
			41.9

Table 3.3 represents the comparison of branch losses for the 4-bus network. As the branch losses are directly related to  $T_c$  and resultant line resistance, Case A has the highest branch loss for individual lines compared to the other cases. For Case C, branch losses for each segment of a line are added together to obtain the total branch loss of respective branches.

Table 3.3: Branch Losses for 4 Bus Network

Branch #	Conventional PF Case A (MW)	Proposed TD-PF Case B (MW)	Difference between Case A and Case B	Proposed TD-PF with TD-LM Case C (MW)	Difference between Case A and Case C
1	11.36	10.945	3.65%	10.74	5.46%
2	3.98	3.85	3.27%	3.8	4.52%
3	1.34	1.29	3.73%	1.3	2.98%
4	8.25	7.83	5.09%	7.76	5.94%
5	1.84	1.80	2.17%	1.79	2.72%

### 3.4.2 39-Bus System

The IEEE 39-bus network is considered in this case study. All lines are Rook type conductor. Out of the 46 branches in the system, only the ones under the yellow shaded region in Fig. 3.5 have weather measurements stations on or near it. Three approaches described as Case A, B and C in the 4-bus case study, are also used for the 39-bus system. Table 3.4 contains the complete weather station locations and measurements.

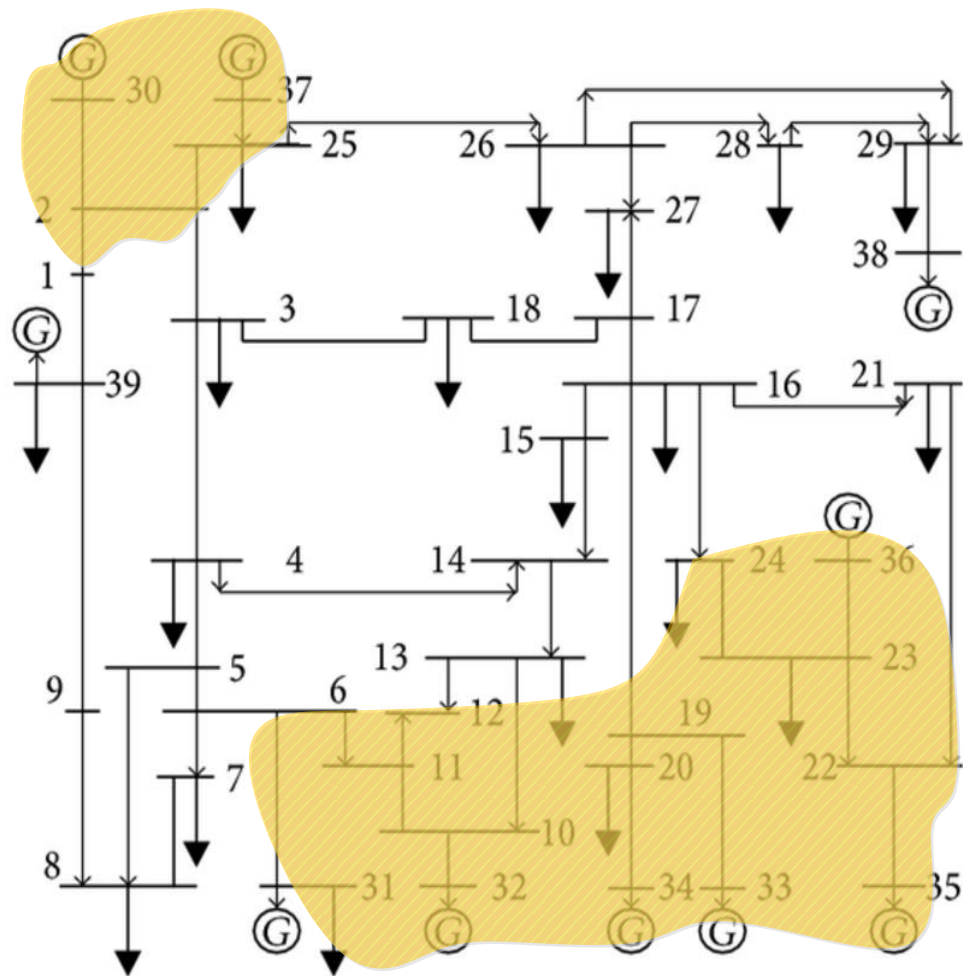


Figure 3.5: 39-Bus System

Table 3.4: Measured Wind Speeds and Ambient Temperatures for 39-Bus System

Branch #	Branch (From-To)	Branch Length (km)	Weather measurement location (from 'From' bus (km))	Wind speed, $v_w$ (m/s)	Ambient Temperature, $T_a$ (°C)
1	1 – 2	80	0, 80	2.3, .85	32, 32
5	2 – 30	70	0, 30, 70	.85, 2.7, 3.6	32, 32, 34
14	6 – 31	80	0, 40, 80	2.9, 2, 1.2	33, 33, 33.5
20	10 – 32	60	0, 60	1.75, 1.2	31, 32
33	19 – 33	80	0, 50	3.4, 2, 0.9	33, 34
34	20 – 34	100	0, 60, 100	2.9, 1.7, 0.75	31, 33, 31
35	21 -22	80	0, 30, 60, 80	5.6, 4.4, 1.8, 1.1	32, 32, 32.5, 31
37	22 -35	80	0, 80	1.1, 2.1	31, 33
38	23 – 24	70	0, 30, 70	3, 2.2, 1.1	32, 32
39	23 – 36	80	0, 80	3, 5	32, 33
41	25 – 37	70	0, 70	0.8, 2.2	34, 33
46	29 - 38	90	0, 50, 90	2.2, 3.1, 4.6	34, 32

Similar to the 4-bus system  $T_c$  for the selected lines in the 39-bus system were higher for Case A, compared to Cases B and C. Table 3.5 presents  $T_c$  for select branches for the three different approaches for the 39-bus system.

Table 3.5: Comparison of Conductor Temperatures for 39 Bus Network

Branch #		Conventional PF Case A (°C)	Proposed TD-PF Case B (°C)	Proposed TD-PF with TD-LM Case C (°C)
To	From			
1	2	75.03	68.8	57.8
				63.8
				66.9
2	30	81.2	74	66.5
				70.9
				73.4
10	32	79.7	68.5	65.8
6	31	74.5	64.8	58.7
				61.2
16	24	55.3	55	53
22	35	77.6	69	49
				61.2
				65.7
23	24	70.8	63	53.6
				57.6
25	37	71.8	66.8	61.6
				57.3

## CHAPTER 4: TEMPERATURE-DEPENDENT TRANSMISSION CAPACITY ANALYSIS

### 4.1 Overview

As the proposed temperature-dependent power flow method provides information about both thermal and electrical conditions of a power system, it has the potential to be utilized in the determination of maximum power handling capability of a system. The proposed algorithm offers the simultaneous comparison of the line currents to reach the thermal and voltage stability limit to determine the critical limiting factor for a transmission network. The highlights of this section can be shown as:

- Utilizing the temperature-dependent power flow for simultaneous determination of thermal and voltage stability limits,
- Development of a temperature-dependent continuation power flow (TD-CPF) method

### 4.2 TD-PF for Transfer Capacity

The proposed power flow approach incorporated with the longitudinal variation of weather conditions delivers the steady-state thermal conditions of transmission lines. Subsequently, its application can inform users if lines are close to their thermal limit. It also provides a more accurate representation of the electrical line parameters, which impacts the determination of the voltage stability conditions of the system. In order to determine the effective power transfer limit of a system, both of the limiting factors need

to be considered. Continuation Power Flow (CPF) provides the maximum power transfer capability of a system based on voltage stability limit [64]. Each line current corresponding to the maximum loading point ( $\lambda_{max}$ ) in CPF is determined and compared to the line current needed to reach the line thermal limit ( $T_c^{max}$ ) under the given weather conditions to determine the critical power transfer limiting factor.

Let,  $I_{i-j(\lambda_{max})}$  = line current to reach  $\lambda_{max}$ , and  $I_{i-j(T_c^{max})}$  = line current to reach  $T_c^{max}$ ,

If ( $I_{i-j(\lambda_{max})} > I_{i-j(T_c^{max})}$ ),

Then Critical limiting factor = Thermal limit

Else Critical limiting factor = Voltage stability limit

#### 4.2.1 Algorithm

The loadability limiting factor for each line, and therefore for the whole transmission system, can be defined, as shown in Fig. 4.1.

Conventionally, maximum loading parameter ( $\lambda_{max}$ ) is used to represent the voltage stability limit of the system using CPF. In this work, a new parameter named ‘effective maximum loading parameter’ ( $\lambda_{max}^{eff}$ ) is introduced in order to incorporate the thermal limit with the voltage stability limit of a transmission system. Though CPF does not provide conductor temperature ( $T_c$ ), the line currents for each step increase in loading parameter,  $\lambda$ , are obtained and then used in the HBE (1) to get the respective  $T_c$ . As the system load is gradually increased during the CPF, the line currents increase at each step, affecting  $T_c$ . The value of the loading parameter,  $\lambda$ , for which the  $T_c$  of a line reaches its maximum allowable conductor temperature ( $T_c^{max}$ ), is the effective maximum loading parameter for the system. The procedure can be summarized as below:

If  $(T_c(\lambda_{max}) < T_c^{max})$

Then  $\lambda_{max}^{eff} = \lambda_{max}$

Else  $\lambda_{max}^{eff} = \lambda(T_c^{max})$

When a transmission line is divided into multiple segments, different segments will have different conductor temperatures. In that case, the segment reaching the maximum allowable conductor temperature first is considered for determining the line thermal limit.

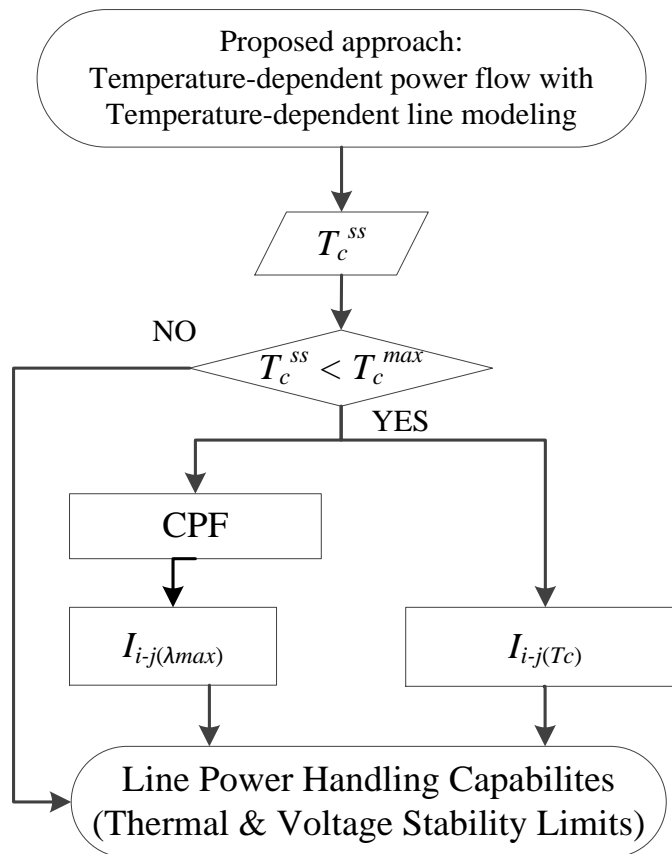


Figure 4.1: Power handling capability studies using temperature-dependent power flow

### 4.3 Case Study Considering Thermal and Voltage Stability Limit

The abovementioned three different approaches result in different line electrical parameters for the 4-bus system. In order to study the impact of the weather conditions on the power handling capability of the system, continuation power flow (CPF) is used on the cases above. Fig. 4.2 shows that for Case C, the value of the maximum loading parameter,  $\lambda_{max}$ , is the highest since segment conductor temperatures are lower than the corresponding  $T_c$ 's for Case A and Case B. For Case A the value of  $\lambda_{max}$  is substantially lower than Cases B (~3%) and C (~4.4%). Table 4.1 shows the tabulated form of the results from the CPF.

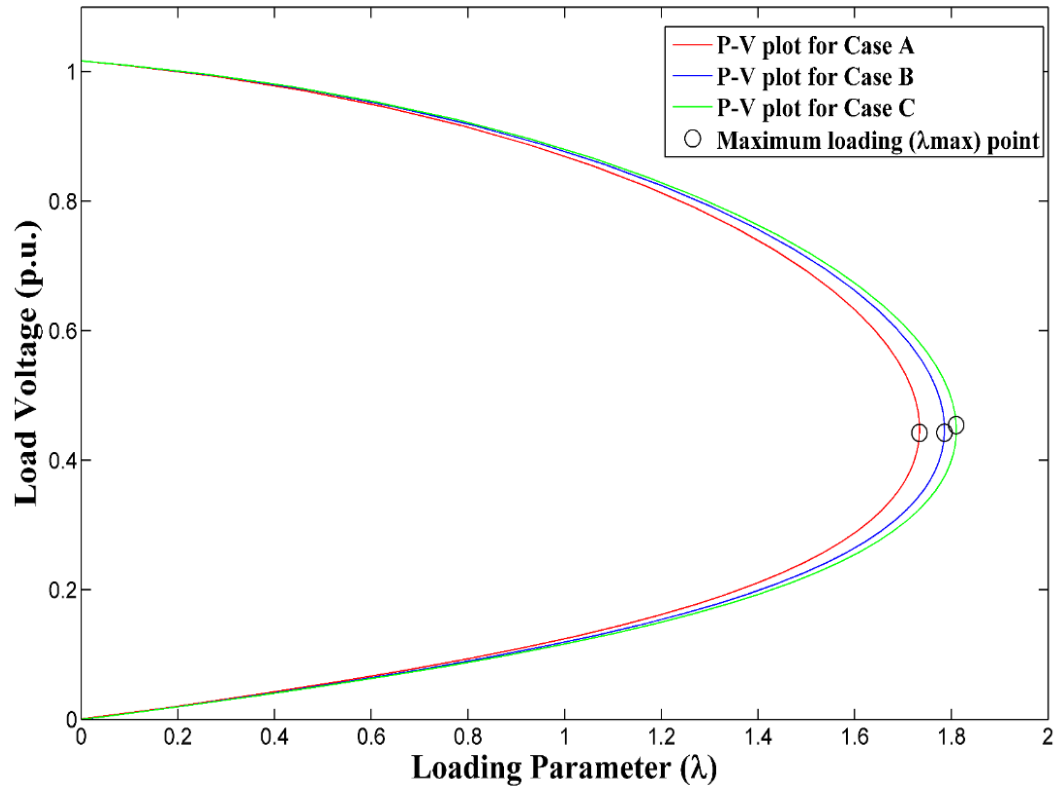


Figure 4.2: P-V plots for bus 2 for each case of the 4-bus system

Table 4.1: Comparison of  $\lambda_{max}$  (4-bus system)

Case #	$\lambda_{max}$	% diff in $\lambda_{max}$ from case A
Case A	1.7340	-
Case B	1.7855	2.97
Case C	1.8100	4.38

Table 4.2 shows the line currents when the system reaches the voltage stability limits, as well as the line currents for individual lines to reach the thermal limits. For all the cases, the branch 1 and branch 4 line currents required to reach the thermal limit are lower than the currents required to reach the voltage stability limit,  $\lambda_{max}$ . Therefore, branch 1 and branch 4 will reach their individual thermal limits before the system reaches  $\lambda_{max}$ . Using the approach discussed in Section 4,  $T_c$  at each step of CPF is calculated. In Fig. 4.3, the asterisk marks (\*) indicate the loading point for which at least one branch of the system reaches  $T_c^{max}$ . However, it must be noted that line currents required to reach thermal limits are not the same for different cases. For conventional power flow (Case A), the system reaches the maximum power handling point whenever the line current for branch 1 or 4 reaches 850 amps, even though according to CPF, branch 1 and 4 can carry line currents of 1163 and 1213 amps respectively. Therefore, for Case A the transmission system cannot reach the point of  $\lambda_{max}$ . The value of  $\lambda$  for which the  $T_c$  for branch 1 or 4 reaches  $T_c^{max}$  would effectively be the  $\lambda_{max}$ . The effective  $\lambda_{max}$ , ( $\lambda_{max}^{eff}$ ) for Case A is found as 1.595.

Table 4.2: Line Currents to Reach Thermal and Voltage Stability Limits

Branch #	Case A		Case B		Case C	
	(I for $\lambda_{max}$ )	(I for $T_c^{max}$ )	(I for $\lambda_{max}$ )	(I for $T_c^{max}$ )	(I for $\lambda_{max}$ )	(I for $T_c^{max}$ )
1	1163	850	1165	980	1182	1100
2	727	850	738	960	740	1000
3	378	850	376	980	377	1110
4	1213	850	1213	1080	1230	1170
5	470	850	470	1065	480	1135

Similar outcomes are obtained for Cases B and C. The line currents required to reach the  $T_c^{max}$  are higher in Case B than in Case A. In Case B, the system reaches its maximum loading point when branch 1 current reaches 980 amps or branch 4 current reaches 1080 amps. The  $\lambda_{max}^{eff}$  for this case is obtained as 1.715, which is 7% higher than the case where measured weather conditions are not taken into account. Furthermore, for Case C, where the longitudinal variation of weather conditions is taken into account the value of  $\lambda_{max}^{eff}$  is the highest, and it is more than 12% higher than that of case A. Table 4.3 shows the comparison among the  $\lambda_{max}^{eff}$  values for three different cases.

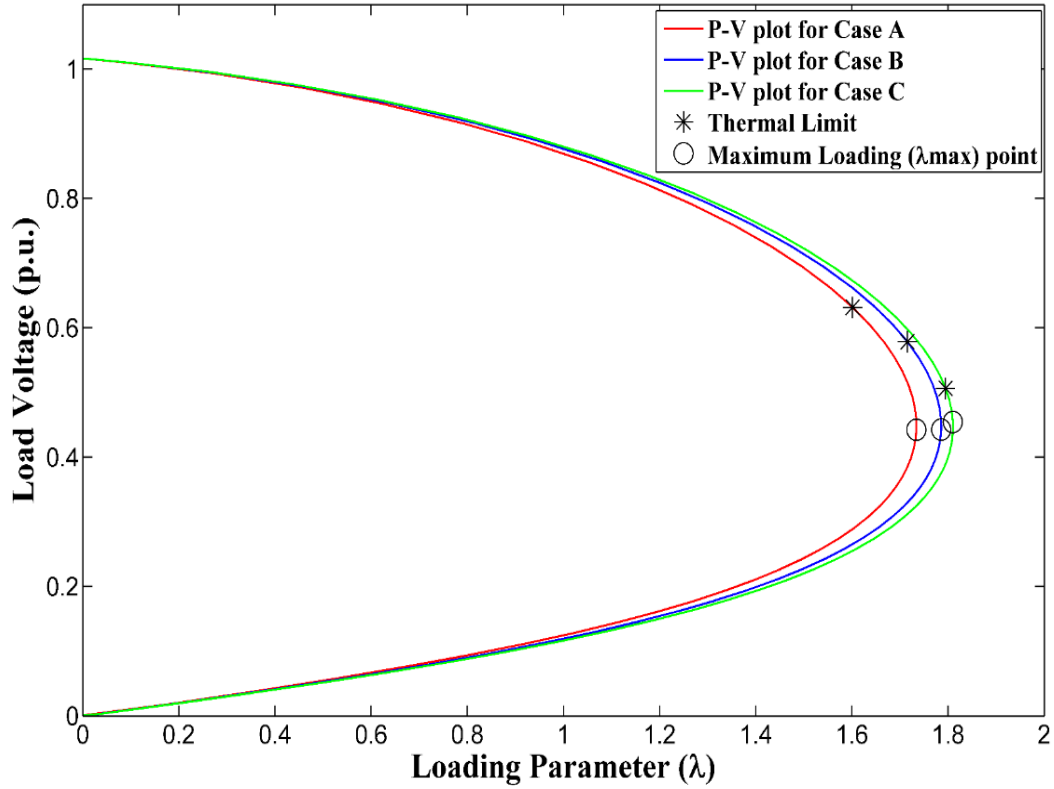


Figure 4.3: P-V plots with thermal limits

Table 4.3: Comparison of  $\lambda_{max}^{eff}$  for 4-Bus System

Case #	$\lambda_{max}^{eff}$	% diff in $\lambda_{max}^{eff}$ from case A
Case A	1.595	-
Case B	1.715	6.99
Case C	1.7925	12.38

#### 4.4 Temperature-Dependent Continuation Power Flow

In conventional continuation power flow the system load is increased gradually until an operating limit is encountered. In this method, the variation in line conductor temperature with the continuous increase in system load and resulting line current is not taken into account. Therefore, the transmission line electrical parameters are also

considered fixed throughout the process, as these parameter are directly dependent on the line conductor temperature. However, change in line current affects the conductor temperature of a transmission line, which impacts the line electrical parameters. This approximation of constant values of electrical parameters throughout the continuation power flow introduces a quantifiable error in the calculation of power handling capability of the transmission lines.

A temperature dependent model of the continuation power flow method (TD-CPF) is developed in this work. This modified version of the CPF takes into account the variations in line currents with the increase in loading. Therefore, the method considers the continuous change in conductor temperature and the subsequent change in line electrical parameters. The developed TD-CPF method is also capable of determining the power transfer limiting factor of a transmission line by tracking the thermal and voltage stability limits of the line at each step.

#### 4.4.1 Algorithm

At the start of the procedure, the values of the electrical parameters of each line in the system are adjusted for the initial loading conditions. In order to get the most correct value of these parameters, i) Newton-Raphson (NR) power flow is performed and subsequent line losses are calculated, ii) the conductor temperature is determined from the line losses, and iii) the line resistances are updated based on the corresponding conductor temperature using (2). Steps i-iii are performed iteratively until the relative variation between the conductor temperatures for two subsequent iterations is within a specified limit,  $\epsilon$ .

When the correct line parameter values for the base case are obtained, the temperature dependent continuation power flow (TD-CPF) is performed. In this method, the line parameter values are updated with each step increase of the loading parameter, and the resultant  $Y_{bus}$ -matrix is also updated. This is done by determining the current conductor temperature using the line losses corresponding to the applied load. The right most part of the heat balance equation (1) represents the loss of a transmission line. For the determination of conductor temperature, the heat balance equation is solved by a non-linear equation solver [32], [59].

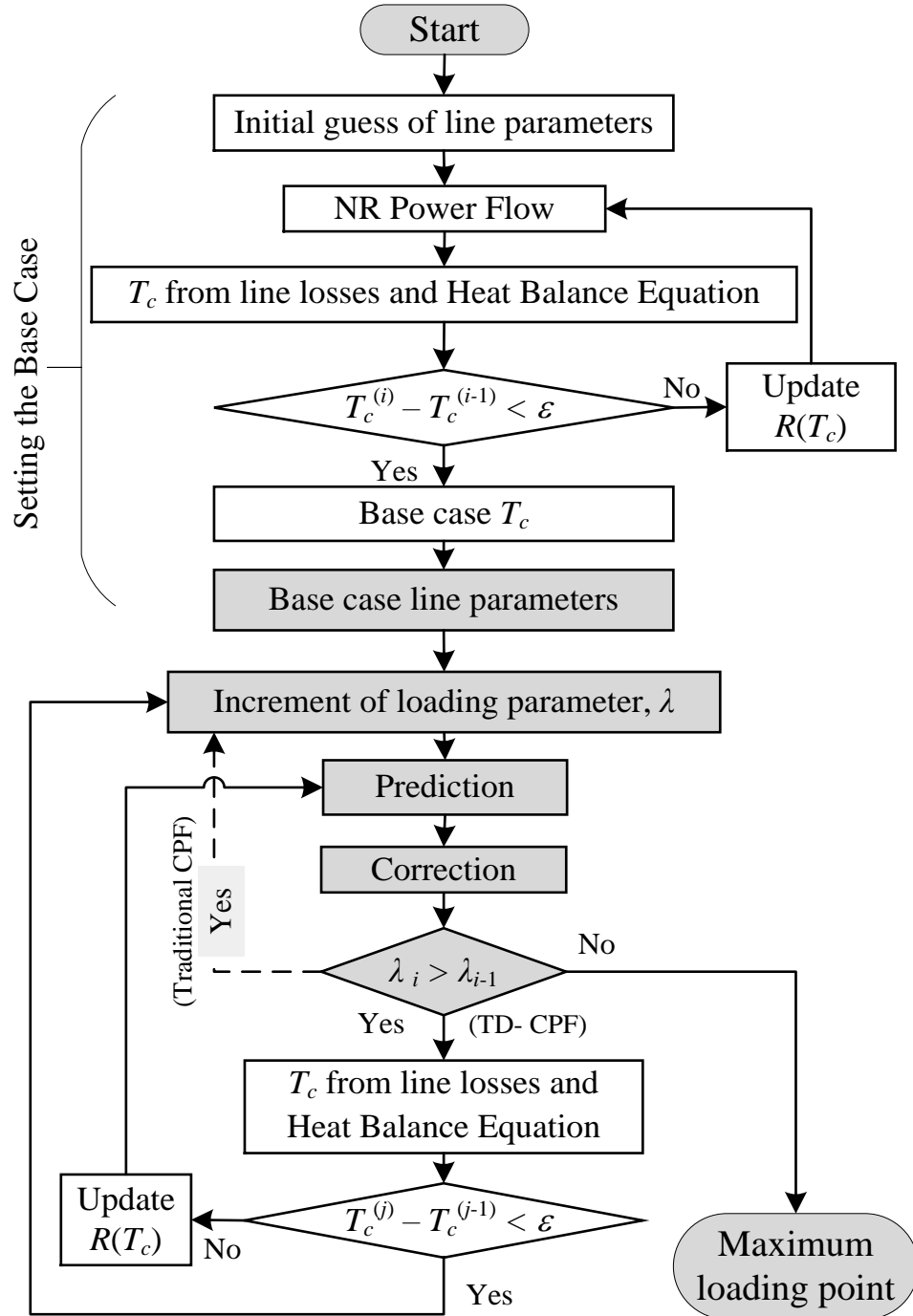


Figure 4.4: Temperature-Dependent Continuation Power Flow

The predictor and the corrector are used multiple times for a same loading parameter to get the correct value of the conductor temperature and resulting line resistance. The iterative process is continued until the conductor temperature between two subsequent iteration steps is within the allowable limit, which in this case was set to  $1 \times 10^{-5}$ .

Prediction and correction with the updated conductor temperature are continued until the value of the loading parameter for a step is not higher than the loading parameter of the previous step, which marks the voltage collapse point for the system. In order to get the full P-V plot, the iteration is continued until the loading parameter,  $\lambda$ , goes back to its initial value. The flowchart in Fig. 4.4 summarizes the TD-CPF procedure.

It is noted that unlike the proposed TD-CPF, conventional CPF does not consider conductor temperature at any point during the determination of the system voltage stability limit. The gray-shaded blocks in Fig. 4.4 highlight the steps of conventional CPF. These blocks show that when the critical point is reached, the loading parameter reaches its maximum value, without considering conductor temperature  $T_c$ . Otherwise, as long as the loading parameter is greater than the previous value, the iterative process continues as showed by the dashed line in the flowchart.

As the conductor temperature is updated at each step of the TD-CPF, the thermal limit of the lines can also be determined using this process. Whenever the conductor temperature reaches the maximum allowable limit, it marks the thermal limit of the transmission line. Between the two power transfer limiting factors of transmission lines – the thermal limit and voltage stability limit, the one which occurs first during this procedure is considered as the main limiting factor for that line.

A new parameter  $\alpha_{max}$  is introduced in this paper to represent the maximum power transfer limit of the transmission line considering both thermal and voltage stability limits. If  $\lambda_{max}$  is the loading parameter to reach the voltage stability limit of the system, and  $T_c^{cri}$  represents the maximum allowable conductor temperature, the maximum power transfer limit of the line can be determined in the following manner:

When,  $k_{\lambda_{max}} < k_{T_c^{cri}}$

$$\alpha_{max} = \lambda_{max}$$

Otherwise, if  $k_{\lambda_{max}} > k_{T_c^{cri}}$

$$\alpha_{max} = \lambda(k_{T_c^{cri}})$$

Where,

$k_{\lambda_{max}}$  = TD-CPF step number to reach  $\lambda_{max}$  and

$k_{T_c^{cri}}$  = TD-CPF step number to reach  $T_c^{cri}$

#### 4.5 Simulation Results

A 120-mile long transmission line is considered for the case studies. The line is made of Drake type conductor [27]. Its maximum allowable conductor temperature is 100°C [14] and the line is located 10 meters above the sea level on a plane land. Five equidistant weather stations are considered along line. At the first measurement location (line sending end), the conductor temperature,  $T_c$ , is 55°C, at location 2 it is 75°C, at location 3 it is 50°C, at location 4 it is 60°C, and at location 5 (line receiving end) it is 50°C. A linear variation of  $T_c$  is assumed between two successive measurement points. The above-mentioned  $T_c$  values at the five measurement locations produce the conductor temperature profile shown in Fig. 4.5.

Based on the above, the transmission line is modeled in two ways: using the multi-segment line modeling approach, and using a single-segment model with parameters calculated at a single conductor temperature. Using an example threshold value of  $15^{\circ}\text{C}$  for the conductor temperature difference between any two points in a segment, a 3-segment line model is obtained. Segments 1, 2 and 3 are 22.5, 25.5, and 72 km long, respectively. The weighted average  $T_c$  for each of the segments are calculated as  $62.5^{\circ}\text{C}$ ,  $65^{\circ}\text{C}$  and  $55^{\circ}\text{C}$ , respectively. A graphical representation of the 3-segment model can be seen in Fig. 4.5. If a single-segment line model is used instead of the multi-segment model, a single value of conductor temperature could be obtained by taking the weighted average  $T_c$  for the entire line, which in this case would be  $60^{\circ}\text{C}$ .

For evaluation purposes, four case studies are considered and compared: 1. conventional CPF and single-segment line model at the single weighted average  $T_c$ , 2. TD-CPF and single-segment line model at the single weighted average  $T_c$ , 3. Conventional CPF and 3-segment line model, and 4. TD-CPF and 3-segment line model. In all cases, the base load on the receiving end of the line is set to 79.4 MVA with a power factor of 0.88.

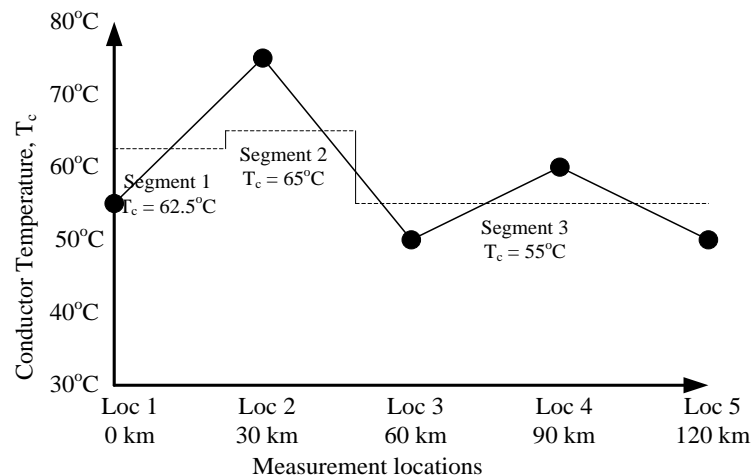


Figure 4.5:  $T_c$  profile and line model segmentation for case 2

*Cases 1 and 3*

when the conventional CPF is applied using a single-segment line model at a single weighted average conductor temperature (Case 1), the maximum loading parameter for the system is found to be 2.6503 marked by the green cross on the plot in Fig. 4.6. However, when the TD-CPF was applied for the same modeling approach (Case 3), the maximum loading parameter is found as 2.6125, marked by the blue dot on the blue line. Therefore, the value of  $\lambda_{max}$  is lower in this case as compared to the conventional CPF, by 1.42%, which is expected as the TD-CPF considers the increase in line resistance with the gradual increase in system load. The red mark in Fig. 4.6 denotes the maximum allowable conductor temperature (100°C). The figure shows that the voltage collapse point for the system occurs before the conductor reaches its maximum allowable temperature. Therefore, voltage stability limit is the main limiting factor in this case for the maximum power transfer capability limit of the transmission line under consideration.

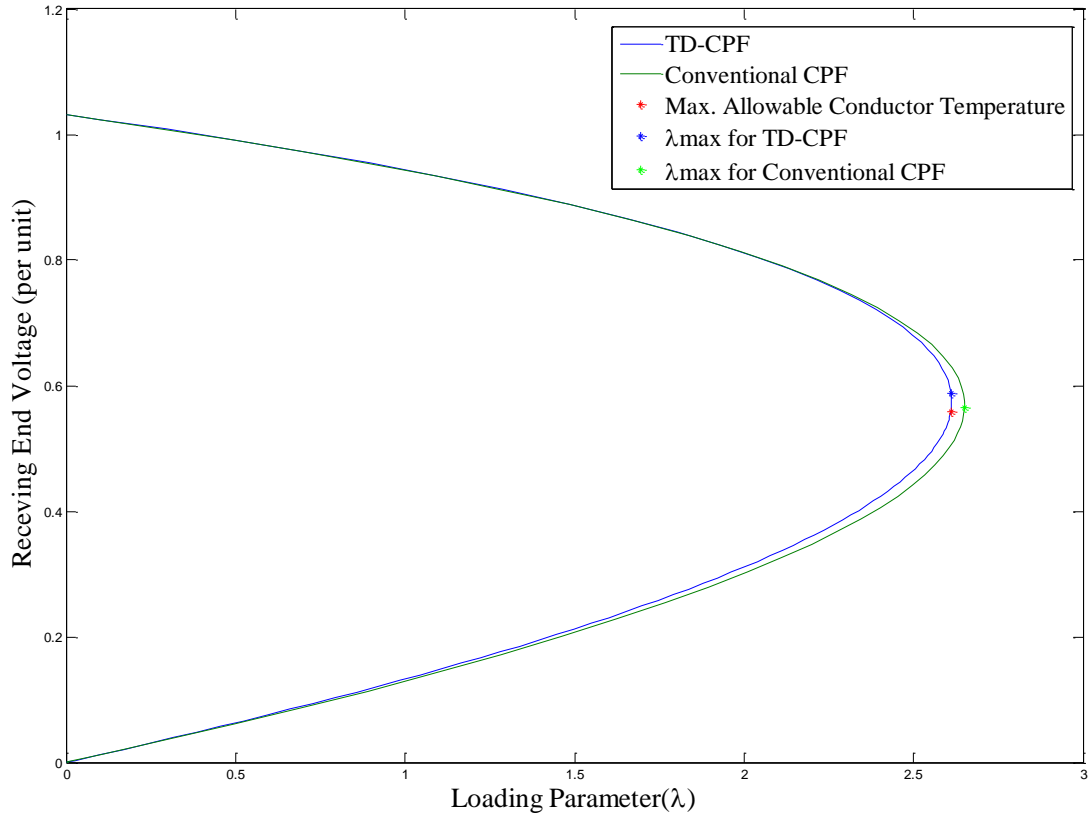


Figure 4.6: Conventional CPF and TD-CPF plots for the single-segment line model at weighted average conductor temperature (Cases 1 and 3)

#### *Cases 2 and 4*

When the conventional and temperature dependent CPF are applied using the 3-segment line model, the plots in Fig. 4.7 are obtained. Three sets of plots in this figure represent the P-V curves for the three segments of the line model. Similarly to the previous case, the maximum loading parameter using the TD-CPF (2.6395) is found to be lower than by using the conventional CPF method (2.6744); this time by 1.31%. In the TD-CPF the conductor temperatures for the three segments do not reach the thermal limit at the same time, as the three segments have different conductor temperatures under the initial loading conditions. For segments 1 and 2, the voltage collapse point, indicated by blue

dots, is reached before the conductor temperature reaches the maximum allowable limit, marked by red dots. However, for segment 3 the thermal limit is reached before the voltage collapse point. As the conductor temperature for each of the segments must be within the limit of the maximum allowable temperature, for this case the thermal limit is the main limiting factor to the line maximum power transfer capability. Though  $\lambda_{max}$  for this case is 2.6395, the conductor temperature reaches 100°C when  $\lambda$  is 2.6304; therefore, the maximum allowable value of the loading parameter for this case is 2.6304.

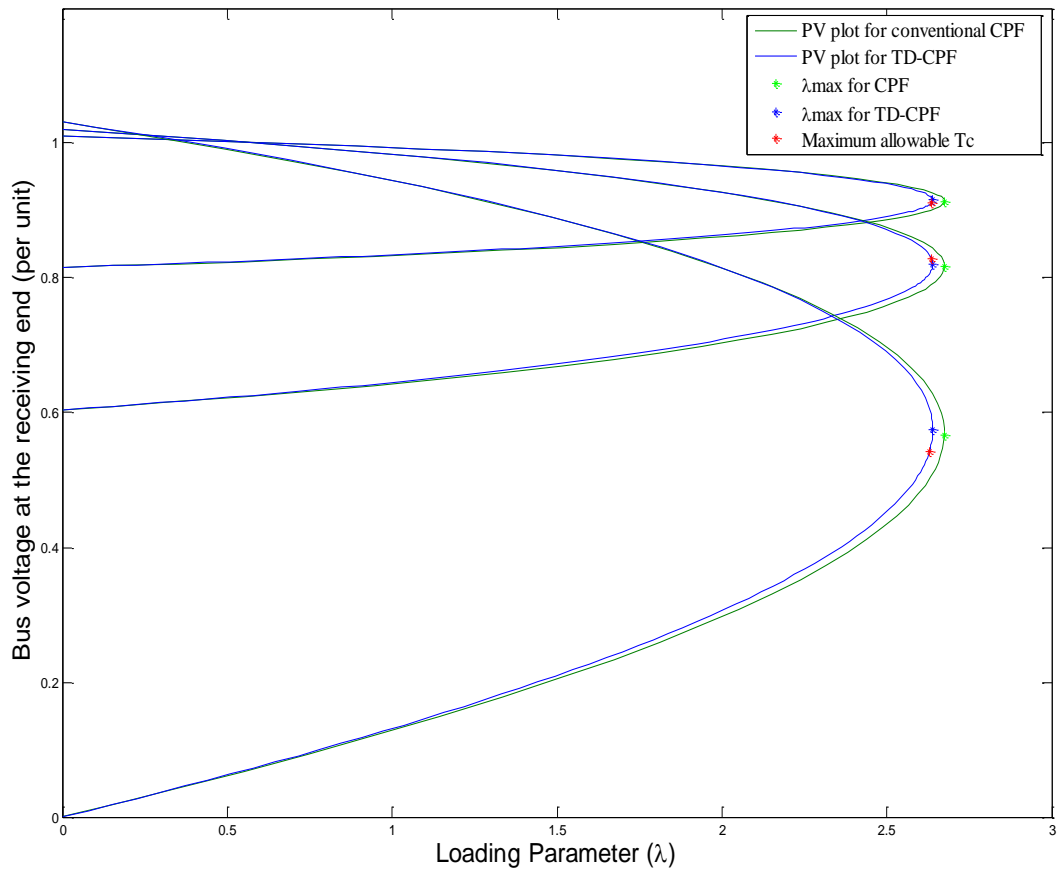


Figure 4.7: Conventional CPF and TD-CPF plots for the 3-segment line model (Cases 2 and 4)

The results from the above mentioned cases are presented in Table 4.4. Conventional CPF cannot provide any information regarding the change in conductor temperature for both the single- and the multi-segment line modeling approaches, as it does not consider the impact of change in line current on the line conductor temperature. Quantifiable differences in  $\lambda_{max}$  are noted among the cases. TD-CPF results in 1.43% lower loadability estimates as compared to the conventional CPF. When the TD-CPF is applied using the single-segment model at a single weighted average conductor temperature (case 3), the voltage stability limit is found to be the main limiting factor as  $T_c$  at  $\lambda_{max}$  is below the thermal limit of 100°C. The  $T_c$  at  $\lambda_{max}$  for the three segments in the multi-segment line modeling approach (case 4) are observed to be 95°C, 103°C and 98°C. The reason behind the higher  $T_c$  on the 2<sup>nd</sup> segment is that the  $T_c$  at that segment was already higher than the other two segments at the initial loading condition. Though the  $T_c$  of segment 1 and 3 are below 100°C at  $\lambda_{max}$ , thermal limit is the limiting factor for maximum power transfer capability for this case as the 2<sup>nd</sup> segment reaches 100°C before  $\lambda$  reaches its maximum value. Therefore, considering both thermal and voltage stability limits, the maximum loading parameter for this case is 2.6304, which is approximately 1.7% lower than the conventional CPF (as seen in the  $\alpha_{max}$  row of Table 4.4).

Table 4.4: Comparison of  $\lambda_{max}$  and  $T_c$  at  $\lambda_{max}$  for Cases 1-4

	Single segment at avg $T_c$			Multi-segment line model			
	CPF	TD-CPF	% diff.	CPF	TD-CPF	% diff.	
$\lambda_{max}$	2.650	2.612	1.43%	2.674	2.639	1.35%	
$T_c$ at $\lambda_{max}$	N/A	95°C	-	N/A	Seg1	96°C	-
					Seg2	103°C	
					Seg3	97°C	
$\alpha_{max}$	2.650	2.612	1.43%	2.674	2.6304	1.69%	

## CHAPTER 5: IMPACT OF DATA UNCERTAINTY ON TEMPERATURE-DEPENDENT POWER SYSTEM ANALYSIS

### 5.1 Overview

Uncertainty in weather parameters arise from different sources, such as solar insolation, ambient temperature, aging, or spatial distribution of climatic variables [65]-[67]. The range of uncertainties may vary with time and location. The uncertainties of these sources can directly impact the branch electrical parameters will not only affect the outputs of the power flow analysis but also have an impact on the maximum power handling capacity of the system [68]-[71]. The goal of this section is to:

- Implement interval arithmetic to account for the data uncertainties in weather conditions;
- Study the impact of the data uncertainties on the power handling capabilities of transmission lines; and
- Integrate interval arithmetic to account for the data uncertainties into the Temperature-Dependent Power Flow method.

### 5.2 Affine Arithmetic (AA) for Data Uncertainty

Affine arithmetic is a modified interval arithmetic approach which is capable of overcoming the limitations interval arithmetic during data uncertainty [72]-[73]. Affine arithmetic can keep the correlations between the input data and computed quantities. This

property of affine arithmetic helps to provide a tighter range in the calculation process by removing the overestimation problem of the standard interval arithmetic method [74]-[75].

The overestimation or wider boundary problem of interval arithmetic can be presented using a simple example –

$$\text{If } f(x) = (8+x)*(8-x), \text{ and } x \in X, x = [-2, +2] \quad (5.1)$$

Interval math gives the total range as

$$8 + X = [6, 10] \quad (5.2)$$

$$8 - X = [6, 10] \quad (5.3)$$

$$(8 + X) - (8 - X) = [36, 100] \quad (5.4)$$

Which denotes the length of the interval is  $100 - 36 = 64$ , while the length of the exact interval,  $[60, 64]$ , is only  $64 - 60 = 4$ . Affine arithmetic approach was introduced as a remedy to this overestimation problem of the interval math. In affine arithmetic, the quantity of a parameter can be presented as [72], [75]

$$\hat{x} = x_0 + x_1\varsigma_1 + x_2\varsigma_2 + \dots + x_n\varsigma_n \quad (5.5)$$

$x_0, x_1, x_2, \dots$  are the floating point real numbers, whose values are known. The  $\varsigma_1, \varsigma_2, \dots$  are called noise variables and can range from -1 to +1. It is to be considered that each  $\varsigma_n$  is independent of the corresponding  $x_n$ . The interval arithmetic,  $\bar{a} = [x, y]$  can be written using the affine form as

$$\hat{a} = a_0 + a_1\varsigma_1 \quad (5.6)$$

$$\hat{a} = \frac{x+y}{2} + \frac{x-y}{2}\varsigma_1 \quad (5.7)$$

### 5.2.1 AA-based Heat Balance Equation

Due to the uncertainties of the input parameters from (3)

$$\hat{T}_a = T_{a0} + T_{a1}\zeta_{Ta}; \text{ Uncertainty of ambient temperature} \quad (5.8)$$

$$\hat{V}_w = V_{w0} + W_{w1}\zeta_{Vw}; \text{ Uncertainty of wind speed} \quad (5.9)$$

$$\hat{\phi} = \phi_0 + \phi_1\zeta_{\phi}; \text{ Uncertainty of Wind direction} \quad (5.10)$$

$$\left. \begin{aligned} \hat{\alpha} &= \alpha_0 + \alpha_1\zeta_{\alpha} \\ \hat{\varepsilon} &= \varepsilon_0 + \varepsilon_1\zeta_{\varepsilon} \end{aligned} \right\}; \text{ Uncertainty from aging, and pollution} \quad (5.11)$$

With respect to (9) the above set of the equations become

$$\left. \begin{aligned} \hat{T}_a &= \frac{T_{a \max} + T_{a \min}}{2} + \frac{T_{a \max} - T_{a \min}}{2} * \zeta_{Ta} \\ \hat{V}_w &= \frac{V_{w \max} + V_{w \min}}{2} + \frac{V_{w \max} - V_{w \min}}{2} * \zeta_{Vw} \\ \hat{\phi} &= \frac{\phi_{\max} + \phi_{\min}}{2} + \frac{\phi_{\max} - \phi_{\min}}{2} * \zeta_{\phi} \\ \hat{\alpha} &= \frac{\alpha_{\max} + \alpha_{\min}}{2} + \frac{\alpha_{\max} - \alpha_{\min}}{2} * \zeta_{\alpha} \\ \hat{\varepsilon} &= \frac{\varepsilon_{\max} + \varepsilon_{\min}}{2} + \frac{\varepsilon_{\max} - \varepsilon_{\min}}{2} * \zeta_{\varepsilon} \end{aligned} \right\} \quad (5.12)$$

In the heat balance equation  $Q_c$ ,  $Q_r$ , and  $Q_s$  – all are dependent on the various external conditions. Therefore, uncertainties in external conditions will introduce uncertainties in conductor temperatures and resultant line electrical parameters. Considering the uncertain values of the external conditions the heat balance equation can be as:

$$Q_c(\hat{T}_a, \hat{v}_w, \hat{T}_c) + Q_r(\hat{T}_a, \hat{\varepsilon}, \hat{T}_c) = Q_s(\hat{\alpha}) + I^2 \hat{R}_{Tc} \quad (5.13)$$

Where,

$T_a$  = Ambient temperature

$v_w$  = wind speed

$\varepsilon$  = emissivity

$\alpha$  = absorptivity

And eventually as:

$$\hat{Q}_c + \hat{Q}_r = \hat{Q}_s + I^2 \hat{R}_{T_c} \quad (5.14)$$

### 5.2.2 Impact of Uncertainties on Line Parameters and Conductor Temperatures

The resulting non-deterministic values of conductor temperatures can affect the line resistance in the following way:

$$\hat{r}_{T_c} = r_{ref} [1 + \alpha(\hat{T}_c - T_{ref})] \quad (5.15)$$

Where

$T_c$  = conductor temperature

$r$  = line resistance

$\alpha$  = temperature coefficient of resistance

$T_{ref}$  = Reference temperature

In an elaborative form (11) can be rewritten as

$$\hat{r}_{T_c} = r_{ref} \left[ 1 + \alpha \left( \left( \frac{T_{c,H} + T_{c,L}}{2} + \frac{T_{c,H} - T_{c,L}}{2} \zeta_{T_c} \right) - T_{ref} \right) \right] \quad (5.16)$$

Where

$T_{c,H}$  = maximum conductor temperature

$T_{c,L}$  = minimum conductor temperature

$\zeta_{Tc}$  = Noise variable for conductor temperature

Apart from the weather conditions, uncertainties in line sag and spacing between line conductors can also affect the values of the line electrical parameters of a transmission line. [76] showed the impact of uncertainties in conductor spacing on the line reactance values using the following equations [63]:

$$\hat{L} = 2 \times 10^{-7} \ln \frac{\hat{d}_{eq}}{r} \quad (5.17)$$

$$\hat{d}_{eq} = \sqrt[3]{\hat{d}_{12} \hat{d}_{23} \hat{d}_{13}} \quad (5.18)$$

Where,

$L$  = inductance

$d_{eq}$  = equivalent spacing

$r$  = conductor radius

Therefore, incorporating the uncertainties into line reactances:

$$\hat{X}_L = 2\pi f \left( \frac{X_{L,H} + X_{L,L}}{2} + \frac{X_{L,H} - X_{L,L}}{2} \zeta_{X_L} \right) \quad (5.19)$$

$$\hat{X}_C = \left( 2\pi f \left( \frac{X_{C,H} + X_{C,L}}{2} + \frac{X_{C,H} - X_{C,L}}{2} \zeta_{X_C} \right) \right)^{-1} \quad (5.20)$$

Where,

$X_L$  = Inductive reactance

$X_C$  = Capacitive reactance

For the representation of the affine forms of the weather parameters under study, historical weather data is required. The weather dataset shown in Table 5.1 was taken at the weather station located at the Charlotte-Douglas International Airport in Charlotte, North Carolina [62].

Table 5.1: Weather Data for summer and winter at 12 Noon

Input data	Summer		Winter	
	Highest	Lowest	Highest	Lowest
Temperature	34°C	25°C	13°C	-2°C
Wind Speed	2.5 m/s	1.4 m/s	2.1 m/s	1.3 m/s

The range of temperature at 12 pm during the summer at the measuring point is from 25°C to 34°C. From (10), the ambient temperature intervals for the line can be expressed as

$$\hat{T}_a = \frac{25 + 34}{2} + \frac{34 - 25}{2} * \zeta_{Ta} \quad (5.21)$$

If the noise variable  $\zeta_{Ta}$  is selected as a vector ranging from -1 to +1, with a regular interval of 0.25, then

$$\hat{T}_a = 29.5 + 4.5 * [-1 : 0.25 : +1] \quad (5.22)$$

Similarly, the affine form for the wind speed:

$$\hat{V}_w = 1.95 + 0.55 * [-1 : 0.25 : +1] \quad (5.23)$$

In Fig. 5.1, red indicates a high conductor temperature and blue low conductor temperature. The figure shows that the wind speed has a stronger impact on conductor temperatures of overhead lines than ambient temperature. A similar type of plot can be drawn for conductor temperature as function of wind direction, solar heat gain, aging, and environmental pollution.

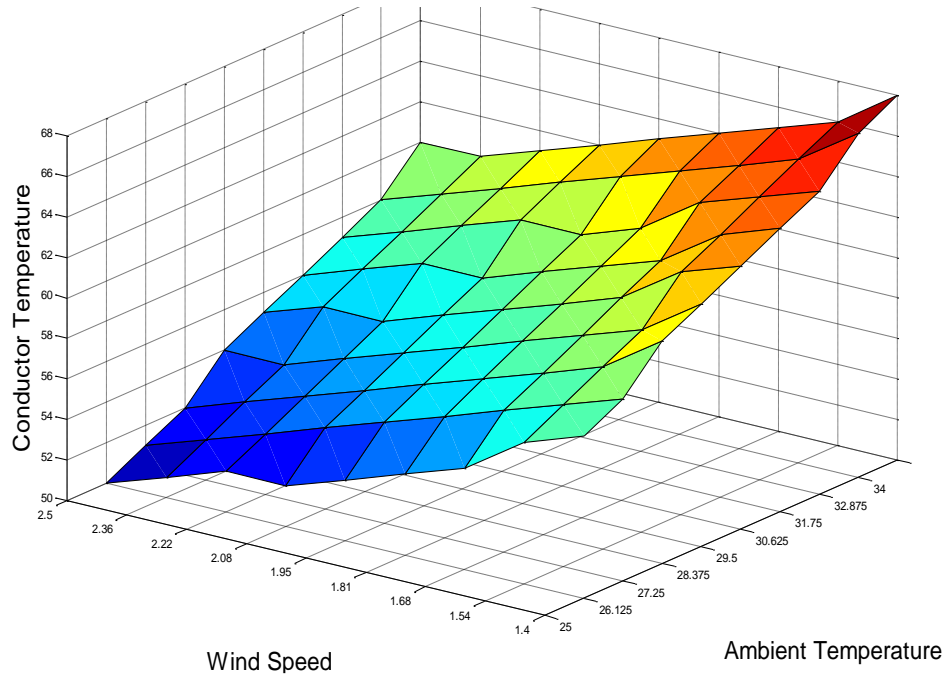


Figure 5.1: Conductor temperature as a function of ambient temperature and wind speed during the summer season

### 5.3 AA-based Temperature-Dependent Power Flow

The goal of this subsection is to investigate the impacts of the uncertainties of ambient conditions on power flow analysis using affine arithmetic and a proposed temperature-dependent power flow method. The developed approach is capable of providing an accurate representation of the electrical and thermal conditions of a system considering the impact of external uncertainties, viewed as intervals, on the branch parameters.

Conventionally used power flow methods do not consider the impact of ambient conditions on the values of the branch electrical parameters and cannot provide information about the thermal conditions of the transmission lines of a system. However, external conditions can have an impact on the branch electrical parameters and eventually can affect the power flow results.

As the elements of the bus admittance matrix is composed of the branch electrical parameters, and line resistances are dependent on the conductor temperatures, therefore the elements of the bus admittance matrix are directly dependent on the conductor temperature. Considering the uncertainties in weather conditions and its impact on the conductor temperatures, the power flow equations can be presented as:

$$\begin{aligned}\hat{P}_i(V, \delta) &= |\hat{V}_i| \sum_{j=1}^n |\hat{Y}_{ij}(\hat{T}_c)| |\hat{V}_j| \cos(\hat{\delta}_i - \hat{\delta}_j - \hat{\theta}_{ij}) \\ \hat{Q}_i(V, \delta) &= |\hat{V}_i| \sum_{j=1}^n |\hat{Y}_{ij}(\hat{T}_c)| |\hat{V}_j| \sin(\hat{\delta}_i - \hat{\delta}_j - \hat{\theta}_{ij})\end{aligned}\quad (5.24)$$

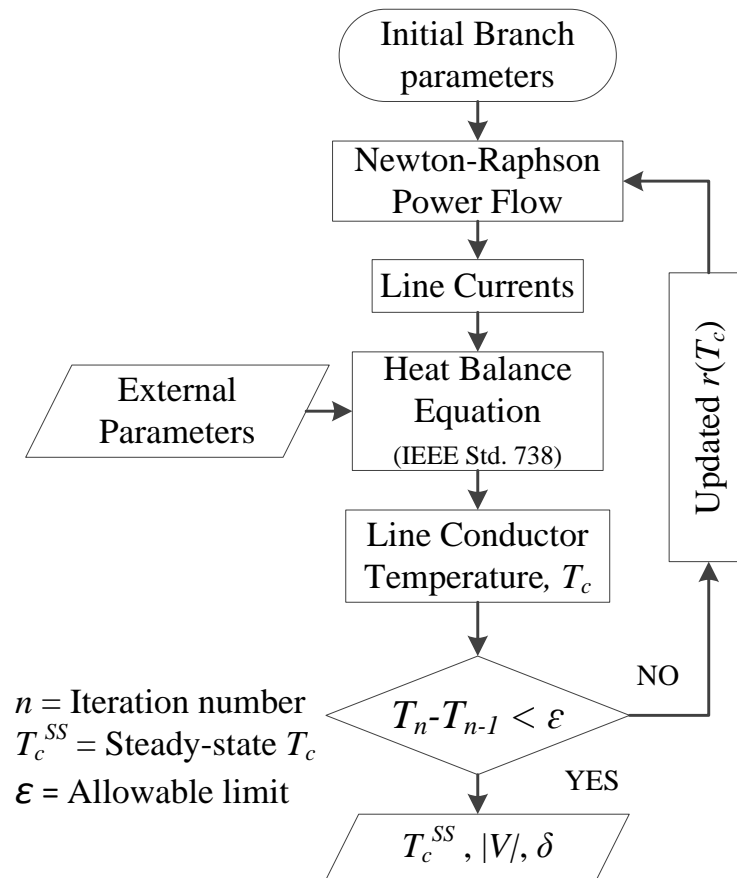


Figure 5.2: Proposed Temperature-Dependent Power Flow with Data Uncertainty

The proposed temperature-dependent power flow takes the external conditions into account, which can often be non-deterministic.

#### 5.4 Simulation Results

##### *4-bus system*

A 4-bus system is considered for the first case study. The system is comprised of 4 transmission lines made of ACSR Rook. The minimum and maximum ambient temperatures and wind speeds are considered for summer and winter for all the branches of the system, from weather measurement data for four different areas from National Oceanic and Atmospheric Administration database [62], as shown in Table 5.2. The length of the branches of the 4-bus system is shown in Fig. 5.3.

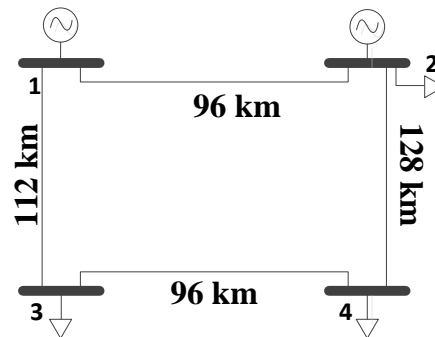


Figure 5.3: 4-bus system

Table 5.2: Ambient temperatures and wind speeds

Branch #	Branch To – From	Ambient Temperature $T_a$ (°C)		Wind Speed $v_w$ (m/s)	
		Summer	Winter	Summer	Winter
1	1 – 2	[18, 39]	[-3, 25]	[.9, 2.8]	[.8, 4.3]
2	1 – 3	[15, 37]	[-2, 26]	[.6, 2.2]	[.8, 2.9]
3	2 – 4	[18, 39]	[-2, 27]	[.6, 3.6]	[.7, 3.1]
4	3 – 4	[17, 37]	[-3, 24]	[.5, 3.3]	[1, 2.4]

Along with the uncertainties in the weather conditions, the uncertainties in line reactance due to variation in line geometry is also considered. According to [77] a +/- 3% variation in the values of the line reactances is used in this case study.

Using the proposed temperature-dependent power flow method integrated with branch parameter uncertainties, the following set of results about the electrical condition of the system was obtained as presented in Table 5.3. Table 5.3 shows that the highest and lowest values of branch losses take place in summer and winter respectively, however, there are times when the branch losses in summer can be lower than the losses in winter. Similar conclusion can be drawn for load bus voltages as well.

Along with the bounds of electrical parameters of the system, the proposed power flow algorithm also provides the range of conductor temperatures ( $T_c$ ) for each branch of the system. The bounds of the conductor temperatures, as shown in Table 5.4, show similar qualitative characteristics to the bounds of the electrical parameters of Table 5.3. Though the upper bounds of the  $T_c$  for summer are much higher compared to those in the winter, at some point the  $T_c$  during summer can be lower than those during winter. This fact highlights the risks/limitations associated with the static seasonal line rating approach, where fixed set of weather conditions are used for line thermal rating for summer and winter seasons [78].

Table 5.3: TD-PF results for 4-bus system

Parameters	TD-PF under external uncertainties (summer)	TD-PF under weather uncertainties (winter)
$ V_2 $ (V)	[0.919, 0.926]	[0.92, 0.928]
$ V_3 $ (V)	[0.881, 0.893]	[0.884, 0.896]
$ V_4 $ (V)	[1.02, 1.02]	[1.02, 1.02]
$\delta_2$ (°)	[-3.233, -3.025]	[-3.065, -3.248]
$\delta_3$ (°)	[-4.315, -4.632]	[-4.356, -4.658]
$\delta_4$ (°)	[4.384, 4.622]	[4.396, 4.653]
$P_{loss12}+jQ_{loss12}$ (MVA)	[2.77+j10.56, 3.168+j11.77]	[2.536+j10.41, 3.013+j11.64]
$P_{loss13}+jQ_{loss13}$ (MVA)	[4.03+j15.4, 4.698+j17.41]	[3.736+j15.18, 4.438+j17.09]
$P_{loss42}+jQ_{loss42}$ (MVA)	[5.298+j20.16, 5.841+j21.4]	[4.998+j20.25, 5.646+j21.51]
$P_{loss43}+jQ_{loss43}$ (MVA)	[9.192+j34.59, 10.42+j37.24]	[8.688+j34.61, 9.833+j37.30]

Table 5.4: TD-PF results for 4-bus system

Branch #	Branch To – From	Conductor Temperature - Summer (°C)	Conductor Temperature - Winter (°C)
1	1 – 2	[29, 56]	[6, 43]
2	1 – 3	[27, 57]	[9, 43]
3	2 – 4	[28, 61]	[9, 48]
4	3 – 4	[32, 70]	[14, 49]

Continuation power flow accounting for different sources of uncertainties of line electrical parameters is performed to study the impact of branch uncertainties on the maximum loadability point of the system. Fig. 5.3 shows the range of the maximum loading parameter,  $\lambda_{max}$ , values for both winter and summer. It can be noticed from the PV plots that at some point the value of  $\lambda_{max}$  for summer uncertainties can be higher than the  $\lambda_{max}$  for winter uncertainties, which is presented by the area where the blue and yellow regions are overlapped. Table 5.5 shows the results from continuation power flow in a tabulated form.

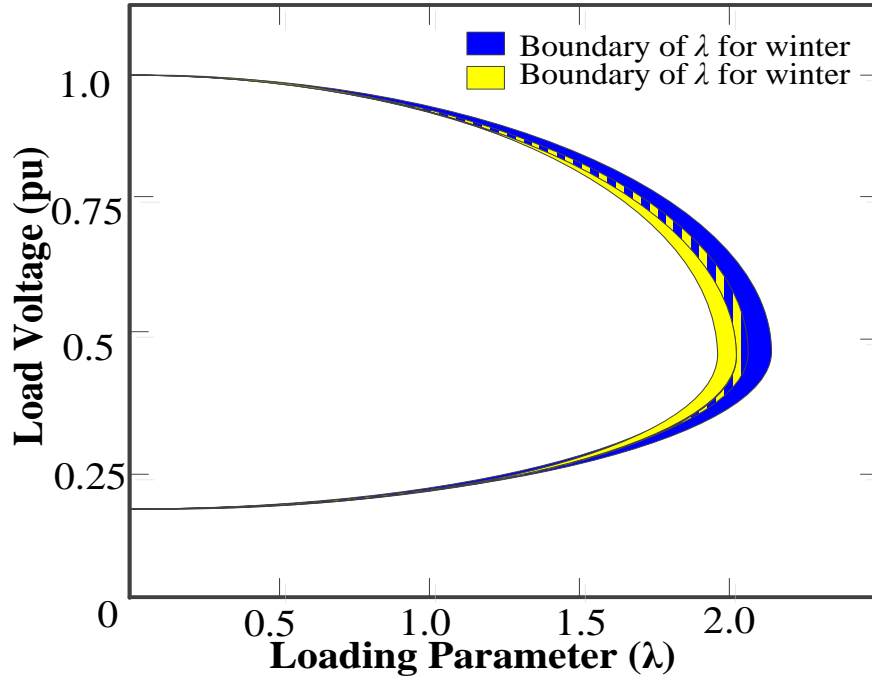


Figure 5.4: PV plot different summer and winter

Table 5.5: TD-PF results for 4-bus system

Season	Maximum loading parameter, $\lambda_{max}$
Summer	[1.85 1.98]
Winter	[1.92, 2.11]

However, voltage collapse point is not the only factor determining the maximum loadability point of a power system network. Thermal limits of the conductor can also play a major role in determining the maximum transfer capability of a system. As the proposed temperature-dependent power flow method is capable of providing information about the thermal conditions of the system, the loading point which causes a branch conductor temperature to reach the maximum allowable limit ( $T_{cmax}$ ) can also be determined from the continuation power flow. Table 5.6 shows the values of  $T_c$  at the  $\lambda_{max}$  point. When the value

of  $T_c$  at  $\lambda_{max}$  point is higher than  $T_{cmax}$  ( $100^\circ\text{C}$ ) for at least one branch, thermal limit would be the primary limiting factor for the system at that particular weather condition.

Table 5.6: Comparison of Branch Currents

Branch #	Conductor temperature. $T_c @ \lambda_{max}$ summer ( $^\circ\text{C}$ )	Conductor temperature. $T_c @ \lambda_{max}$ winter ( $^\circ\text{C}$ )
1	[46, 81]	[20, 70]
2	[70, 144]	[51, 112]
3	[37, 75]	[18, 62]
4	[80, 162]	[71, 122]

### *30-bus system*

The affine arithmetic based power flow was also performed on a 2-area 30-bus network presented in Fig. 5.5 [79]. Two sets uncertainties in ambient temperatures and wind speeds for two different areas are considered for this case. The boundaries of uncertainties in the ambient conditions are shown in Table 5.7.

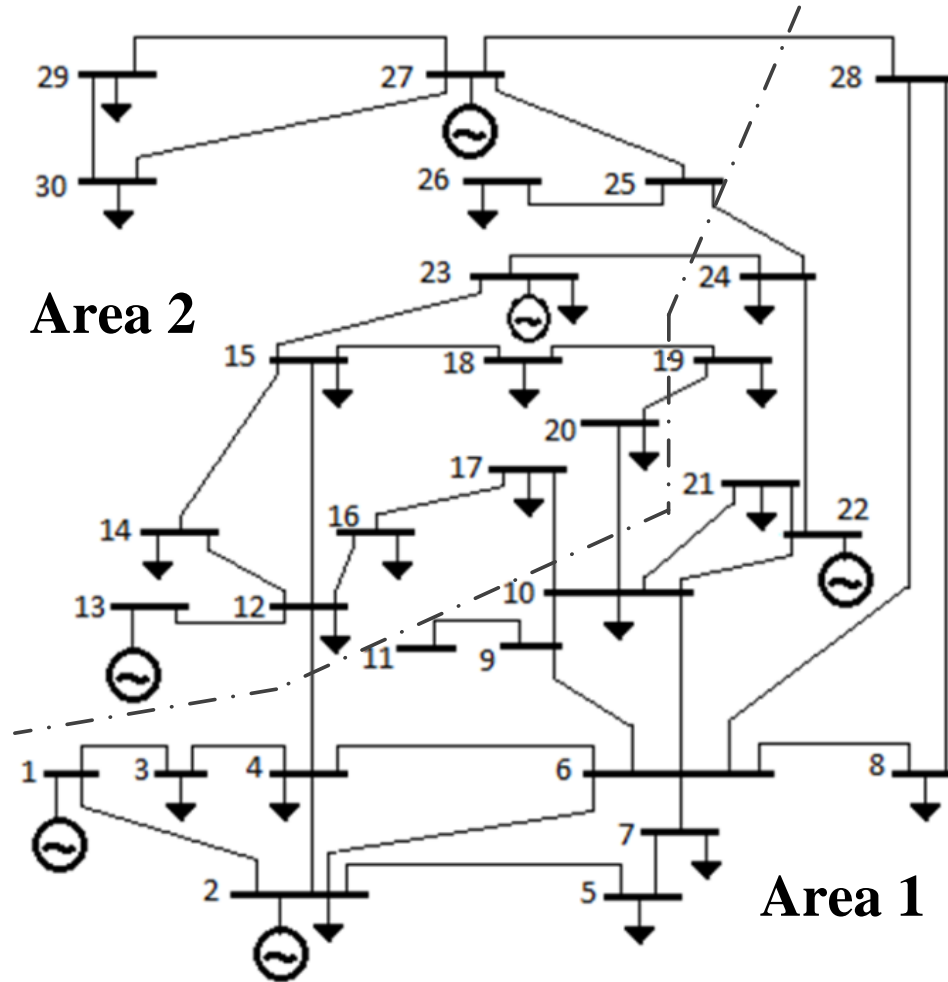


Figure 5.5: Two-area 30-bus system

Table 5.7: Weather data for 4-bus system

Area	Ambient Temperature $T_a$ (°C)		Wind Speed $v_w$ (m/s)	
	Summer	Winter	Summer	Winter
1	[22, 39]	[3, 22]	[.9, 3.1]	[.8, 3.5]
2	[19, 34]	[-2, 20]	[.7, 3.3]	[.8, 2.9]

The power flow results incorporating the line parameter uncertainties are shown in the following figures. Fig. 5.6 shows the boundaries of the voltage magnitudes for winter

and summer conditions respectively. The possible range of conductor temperatures for summer and winter time are presented in Fig. 5.7.

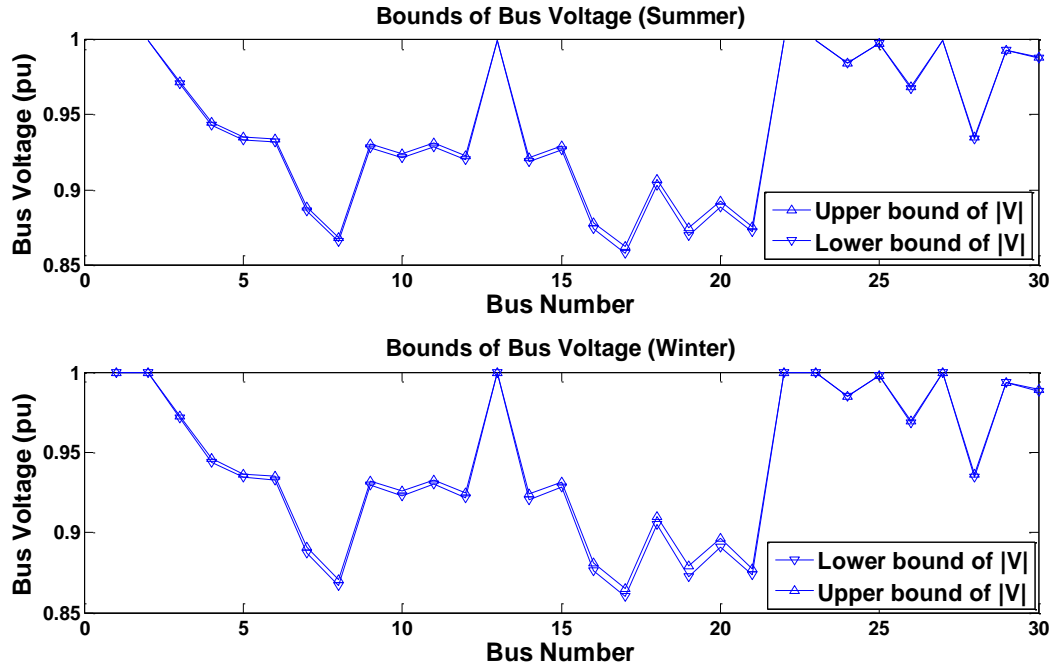


Figure 5.6: Boundary of voltage magnitudes

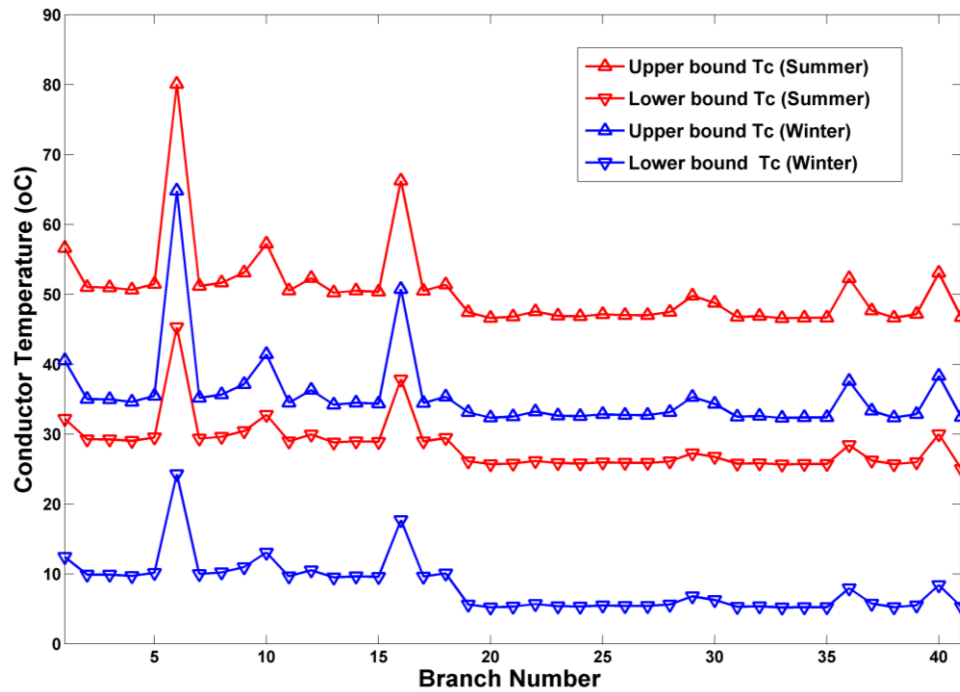


Figure 5.7: Conductor temperatures from proposed TD-PF

Using the continuation power flow approach the boundaries of the maximum power transfer capability point of the 30-bus system can be determined as shown in Fig. 6.8. Similar outcomes compared to the 4-bus case were observed in this case as all. The tabulated form of the PV plots is presented in Table 5.8.

Table 5.8: TD-PF results for 4-bus system

Season	Maximum loading parameter, $\lambda_{max}$
Summer	[5.3, 5.46]
Winter	[5.41, 5.61]

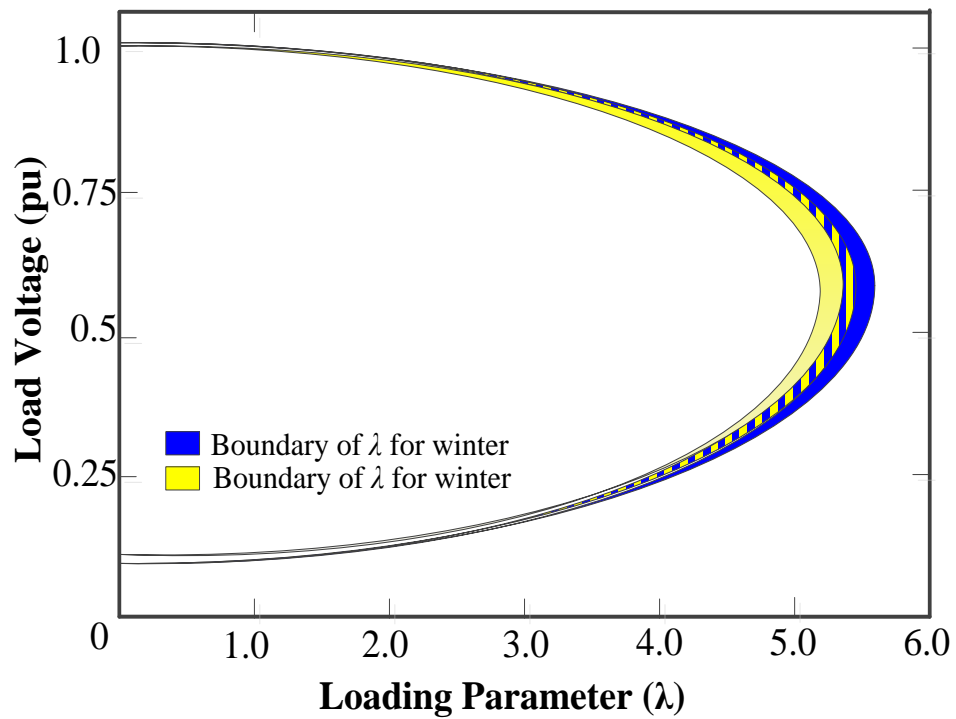


Figure 5.8: PV plot for 30-bus system

## CHAPTER 6: TEMPERATURE-DEPENDENT POWER FLOW COUPLED WITH NON-STATIC HEAT BALANCE

### 6.1 Overview

An overhead transmission line may lose its steady-state thermal conditions when there is a change in weather conditions, variation in system loads or there is an outage of one or more lines in the network [80]. Change in any of the mentioned parameters would affect the conductor temperatures which may impact the line electrical parameters [55], [81]. However, the change in conductor temperature and electrical parameters are not instantaneous, rather it takes place gradually within a certain period of time [32], [81]. During this period of time the thermal and voltage stability limits of a transmission system also change over time until the all the lines reach a new steady-state conductor temperature or the system faces a voltage instability point. This chapter highlights the following points:

- Reviews the impact of the variation in weather parameters or system load or branch outage on the line thermal conditions using non-steady state heat balance equation.
- Development of a time-dependent temperature-dependent power flow algorithm capable of incorporating non-steady-state heat balance conditions.
- Comparing the results of the proposed method with the conventional approach in case of transient thermal conditions.

## 6.2 Non-Steady-State Heat Balance Equation

A conductor experiencing a step change in branch current is then subjected to a gradual change in conductor temperature. The non-steady-state heat balance equation (6.1) can calculate the time required for an overhead line conductor to reach the new steady-state conductor temperature [32].

$$\Delta T = \frac{I^2 r(T) + Q_s - Q_c - Q_r}{mC_p} \Delta t \quad (6.1)$$

In order to obtain the updated conductor temperature after time  $\Delta t$ , the increase in conductor temperature,  $\Delta T$  is added to the previous steady-state conductor temperature:

$$T = T^{ss}_{(old)} + \Delta T \quad (6.2)$$

The value of the updated conductor temperature  $T$  must remain below the maximum allowable conductor temperature,  $T^{max}$ , for safe operation of the transmission line. When rearranged, (2) also provides the time required for the conductor to reach its  $T^{max}$  during a step change in current [56].

The value of  $\Delta t$  for which the updated temperature reaches the thermal limit or a new steady-state conductor temperature is called as critical time,  $t^{crit}$ . The critical time,  $t^{crit}$ , may also indicate the time to reach the voltage collapse point, if the voltage stability limit reaches faster than the thermal limit in a system.

## 6.3 Time-Dependent and Temperature-Dependent Power System Simulation

When there is an outage of a branch in the system or a step change in the system load, the flow of current through one or more branches can change abruptly. The corresponding conductor temperature will continue to rise until it reaches a new steady-

state thermal condition following equation 6.2. The variation in conductor temperature(s) will also affect the voltage stability condition of the system [82]. Thus, for example, a branch contingency can result in either:

- i) updated steady-state thermal and voltage conditions, or
- ii) violation of thermal limits in one or more branches, or
- iii) voltage issues.

In the case of a branch contingency, the power flow through different branches changes immediately (at  $t = 0^+$ ). The change in branch currents impacts the conductor temperatures  $T$  of the respective branches following the non-steady-state HBE:

$$\Delta T_m = \frac{I_m^2 r(T_{m-1}) + Q_s - Q_c(T_{m-1}) - Q_r(T_{m-1})}{mC_p} \Delta t \quad (6.3)$$

where  $m$  is the time step number,  $T_m = T_{m-1} + \Delta T_m$ , and for  $m = 1$ ,  $T_{m-1} = T^{ss}$ .

The gradual change in  $T$  affects line series resistances and changes in branch currents and losses. Therefore, post contingency branch currents are not constant until they reach the new steady-state conductor temperature. The variation in line currents can be obtained from solving the power flow equations at each time-step (10), for bus  $i$ :

$$\begin{aligned} P_i(\delta, V, T) &= V_i \sum_{j=1}^N V_j (G_{ij}(T_{m-1} + \Delta T_m) \cos \delta_{ij} + B_{ij}(T_{m-1} + \Delta T_m) \sin \delta_{ij}) \\ Q_i(\delta, V, T) &= V_i \sum_{j=1}^N V_j (G_{ij}(T_{m-1} + \Delta T_m) \sin \delta_{ij} - B_{ij}(T_{m-1} + \Delta T_m) \cos \delta_{ij}) \end{aligned} \quad (6.4)$$

Therefore, in order to solve for the thermal and electrical conditions of a power system during a branch contingency, both the nonlinear algebraic power flow equations and the difference equation for non-static conductor heat balance are needed.

Thus, in this work, an algebraic-discrete system of equations is adopted. Inspired by a specific subset of differential-algebraic-discrete (DAD) hybrid power systems [83]-[84], the dynamics of conductor temperature are viewed as discretized events and subsequent changes in series resistances are incorporated into switched systems of nonlinear algebraic equations. Compactly, with (11) as  $g$  and (10) as  $z$ :

$$\begin{cases} g_m(x, T) = 0 \\ z(x, T, m) = 0; \text{ given time step } \Delta t \end{cases} \quad (6.5)$$

and the state variables  $x$ , as  $|V|$  and  $\delta$  at each bus, are dependent on the discrete variables  $T$ .

### 6.3.1 Algorithm for the proposed method

The proposed contingency analysis approach is shown in flowchart form in Fig. 2. Following a contingency, a power flow with initial parameters is run to check for convergence, if the power flow does not converge, then static voltage security has been violated [85]-[86]. Else, the updated branch currents are fed into (10) along weather parameters and a preset time-step,  $\Delta t$ , to determine updated conductor temperatures.

If the updated conductor temperature for each branch is below its maximum allowable limit ( $T^{max}$ ), the branch resistance for each transmission line is updated (4). On the other hand, if the calculated conductor temperature reaches its  $T^{max}$ , that branch is considered to have reached its thermal limit and appropriate measures must be taken. Whenever a branch reaches its  $T^{max}$ , its associated power flow becomes one of the power transfer limiting factors for the system.

If none of the limits are reached, then convergence to a new thermally driven steady-state condition is achieved when the difference in conductor temperatures for two successive iterations falls within a set threshold value for each of the branches.

A byproduct of including the time-varying characteristic of the HBE is that the approach also identifies the time taken to reach the resulting end condition mentioned above (i, ii or iii) within  $\Delta t$ . Specifically, an iteration counter is used to track the critical time,  $t^{cr}$  required to reach any of the limits or the new steady-state condition.

Weather measurements may be updated during the process. It is noted if some of the branches have multiple sets of weather condition measurements along its length, the set resulting in the lowest ampacity for that particular branch is used for the proposed method [87]. Temperature-dependent line modeling approaches which consider longitudinal variations in conductor temperatures along a line can also be used [41], [54].

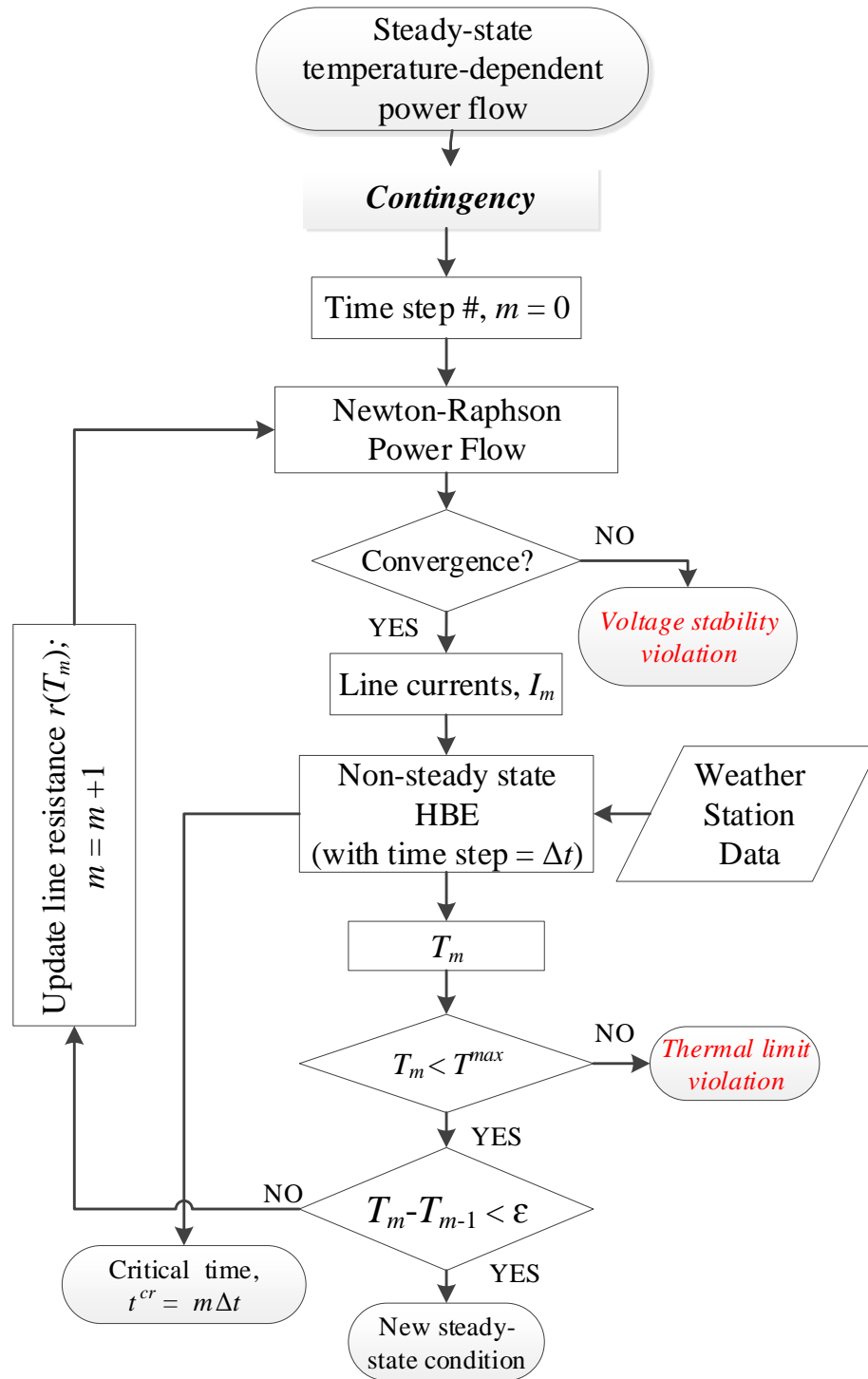


Figure 6.1: Temperature-dependent contingency analysis

## 6.4 Simulation Results

### 6.4.1 2-Bus System

The proposed method is applied to an illustrative 2-bus 2-line system. The results of the proposed method in terms of critical time and limiting factor are compared to those obtained from solely the non-steady-state HBE, without considering the variation in post-contingency line current due to the change in conductor temperature and line impedance, i.e.  $I$  in (9) is not changing with time step  $m$ . In this section, this approach for comparison is referred to as dynamic line rating (DLR) under non-static thermal conditions – DLR for short in result tables and plots. In the following test cases, the tolerances  $\varepsilon_1$  and  $\varepsilon_2$  in Figs. 1 and 2 are set to  $10^{-3}$ .

A 230 kV 2-bus 2-line transmission system is considered (Figure 6.2). Both lines are 75 mile long and are made of ACSR Rook conductor [29] with a predefined line ampacity of 870 A for a  $T^{max}$  of  $100^\circ\text{C}$ . The effects of a line outage for three different loading and weather conditions (Cases A-C) are studied as presented in Table 6.1.

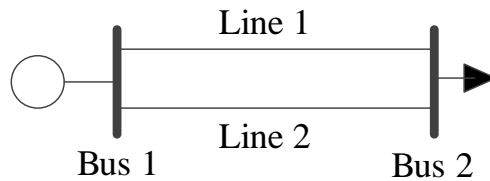


Figure 6.2 : A 2-line 2-bus system

Table 6.1: Loading conditions for the 2-bus system

Bus 2 Loading Conditions:	
Case A	$260 + j102$ MVA
Case B	$265 + j98$ MVA
Case C	$256 + j108$ MVA

*Case A:* Both lines are subjected to the same wind speed (1.2 m/s) and ambient temperature (34°C). The pre-contingency line currents and conductor temperatures are obtained using the proposed temperature-dependent power flow and are shown in Table 6.2.

Table 6.2: Pre-contingency results from TD-PF – Case A

Line	$T$	$I$
1	49.3°C	361 A
2	49.3°C	361 A

Following a line 2 outage, line 1 experiences a step increase in line current (to 1022 A), which results in a gradual rise in conductor temperature  $T_c$ . The change in  $T_c$  following the step increase in line 1 current is plotted in Figure 6.3 for: i) the proposed approach (as described in Figure 6.1, and ii) the DLR approach for non-static thermal conditions, as defined at the beginning of this section. The DLR approach for non-static thermal conditions considers the post-contingency current to stay constant throughout the duration of the increase in  $T_c$ , while the proposed approach accounts for the variation in current, as shown in Figure 6.4. The DLR approach shows that after 43 minutes  $T_c$  reaches a new acceptable steady-state condition ( $T^{ss}$ ), while the proposed method shows that  $T_c$  would reach its allowable maximum,  $T_c^{max}$  of 100°C, after 33 minutes. This is summarized in Table 6.3. The subsequent line 1 real power losses obtained using the proposed method and using DLR are shown in Figure 6.5. It is noted that although current is constant in the DLR approach, the line resistance changes with conductor temperature, causing the real power losses to change with time.

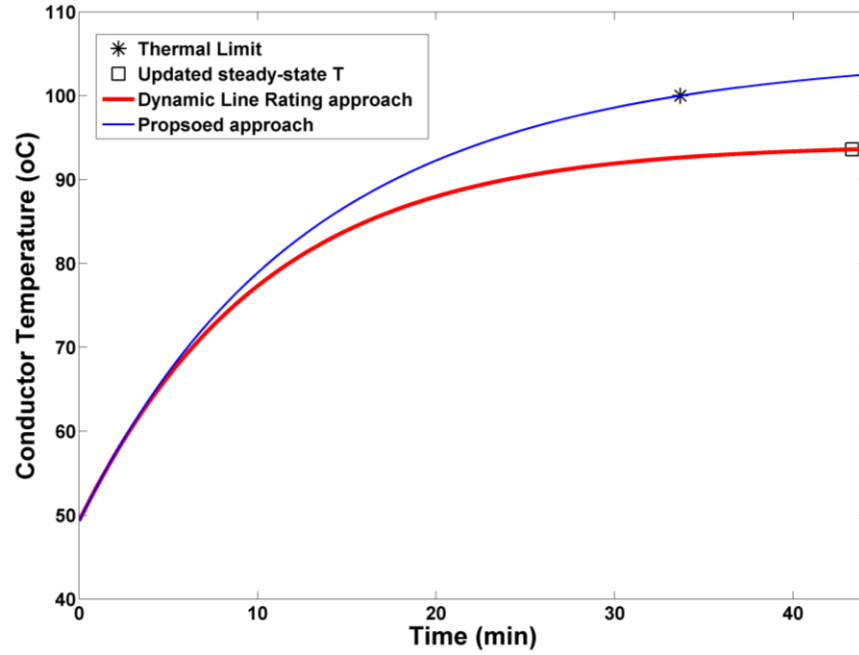


Figure 6.3: Line 1 conductor temperature – Case A

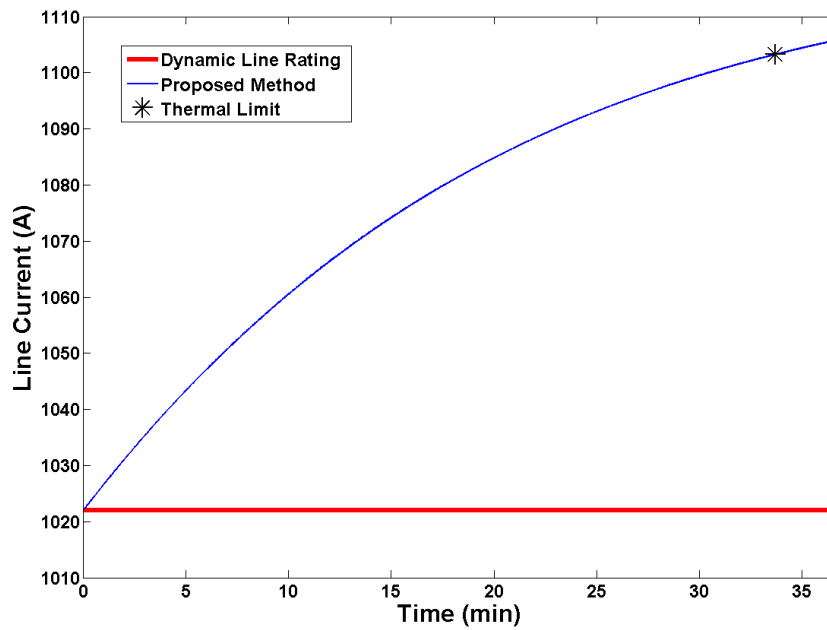


Figure 6.4: Line 1 current – Case A

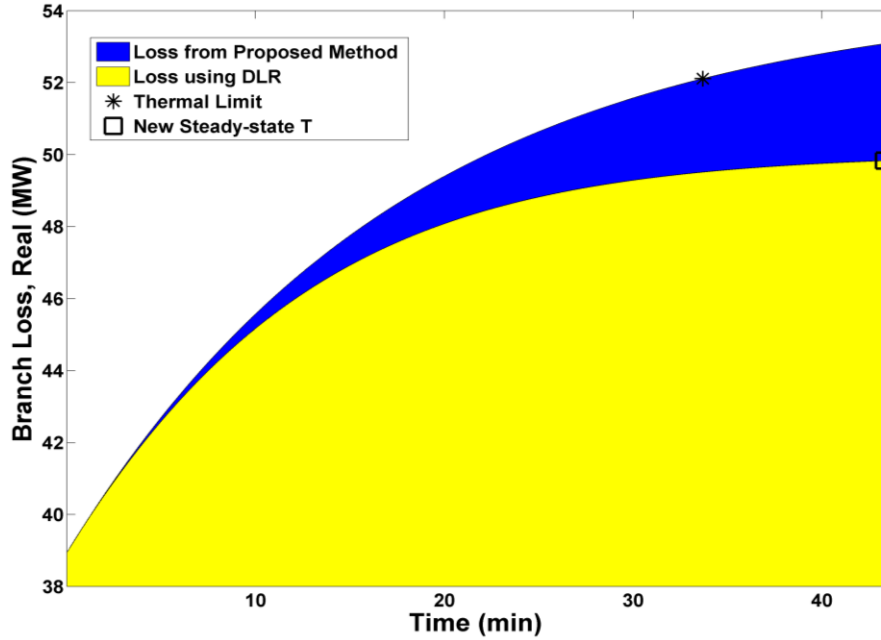


Figure 6.5: Line 1 real power loss – Case A

Table 6.3: Resulting limiting factor and critical time – Case A

	Conventional Method	Proposed Method
Final condition	New steady-state condition (93°C)	Thermal limit
Time, $t^{cr}$	43.3 min	33.7 min

*Case B:* Given the same ambient temperature and a lower wind speed of 0.9 m/s with respect to Case A, for both lines, the pre-contingency conductor temperatures and line currents shown in Table 6.4 are obtained from the TD-PF.

Table 6.4: Pre-contingency results from TD-PF – Case B

Line	$T_c$	$I$
1	51.4°C	365 A
2	51.4°C	365 A

Following a line 2 outage, line 1 current increases to 1033 A. This fixed value of line current is used in the non-steady-state HBE for the DLR approach, while the proposed method considers the increase in  $I$  with time, resulting in the current shown in Figure 6.6. Figure 6.7 then shows the resulting conductor temperature with time; it also shows that the thermal limit,  $T^{max}$ , is reached using the proposed approach after 20 minutes, while using the DLR approach after 30 minutes. The tabulated form of Figure 6.7 is presented in Table 6.5. Line 1 real power loss obtained with both approaches is shown in Figure 6.8.

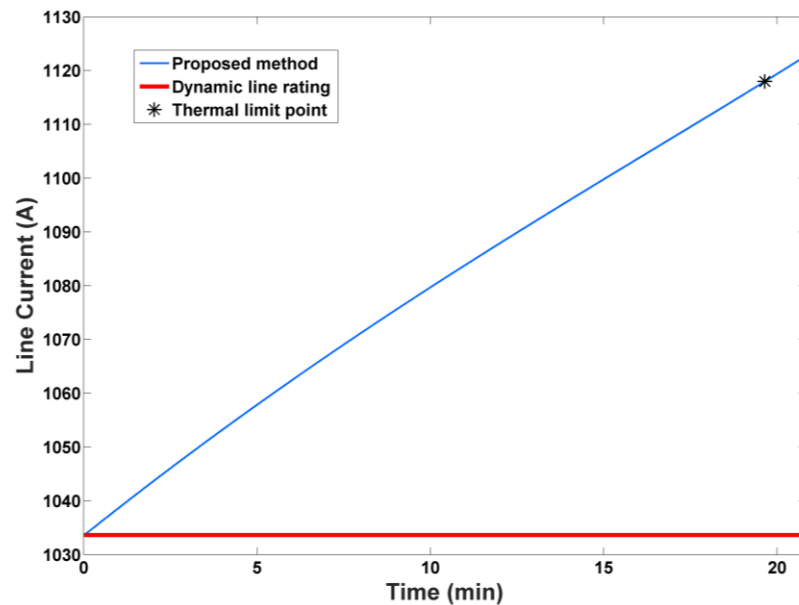


Figure 6.6: Line 1 current – Case B

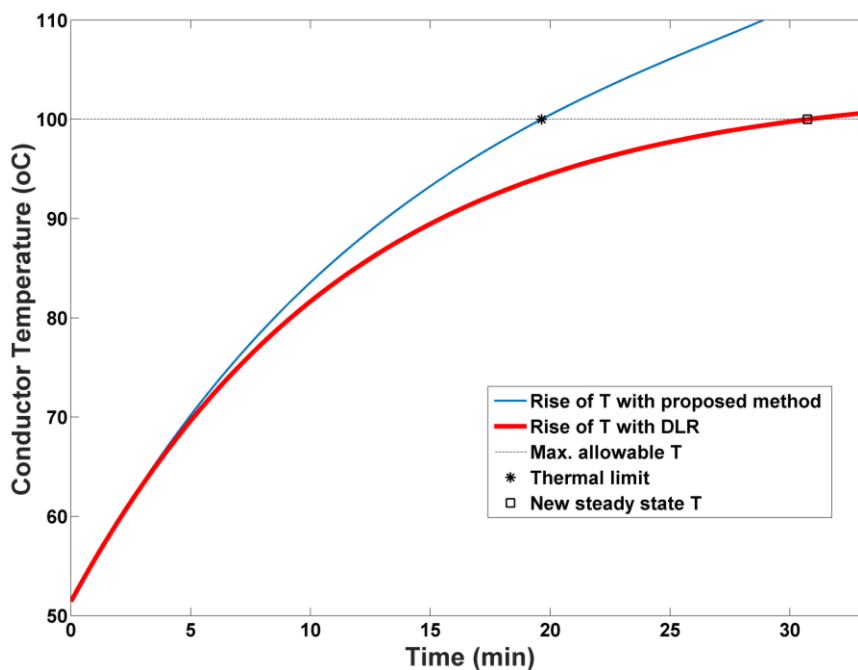


Figure 6.7: Line 1 conductor temperature – Case B

Table 6.5: Resulting limiting factor and critical time – Case B

	Conventional Method	Proposed Method
Final condition	Thermal limit	Thermal limit
Time, $t^{cr}$	30.7 min	20 min

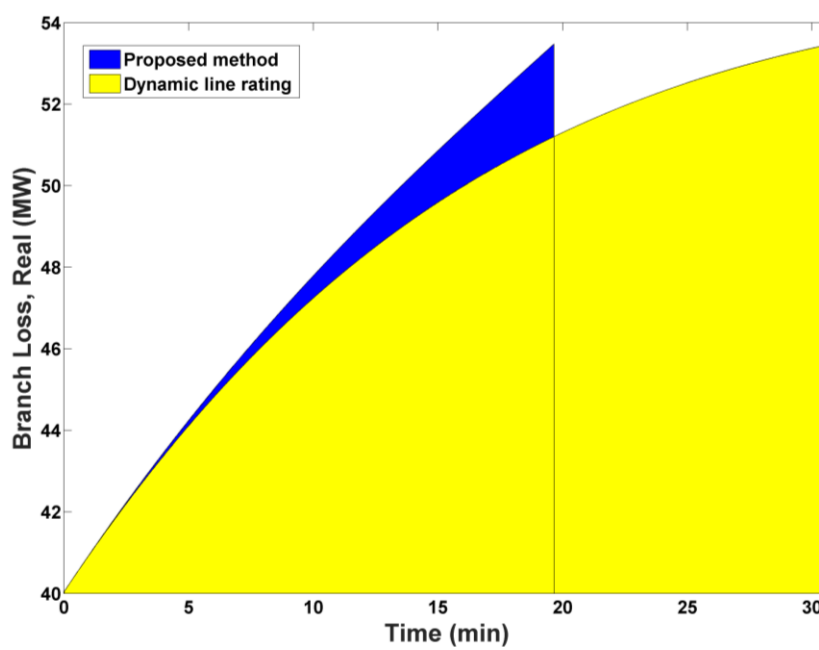


Figure 6.8: Line 1 real power loss – Case B

*Case C:* The same weather conditions as in Case B and a more reactive load as compared to case B are given in this case. The pre-contingency line currents and the conductor temperatures obtained from the TD-PF are shown in Table 6.6.

Table 6.6: Pre-contingency results from TD-PF – Case C

Line	$T_c$	$I$
1	51.1°C	359 A
2	51.1°C	359 A

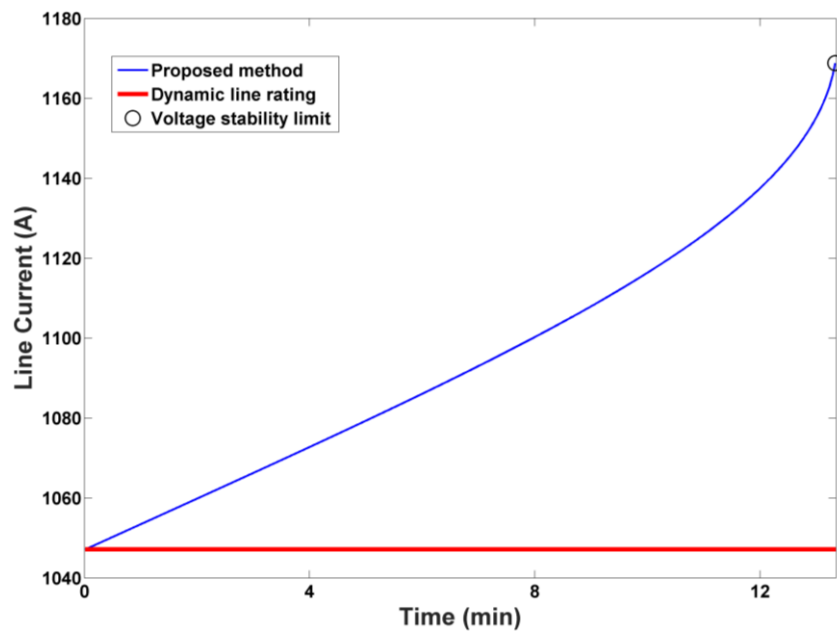


Figure 6.9: Line 1 current – Case C

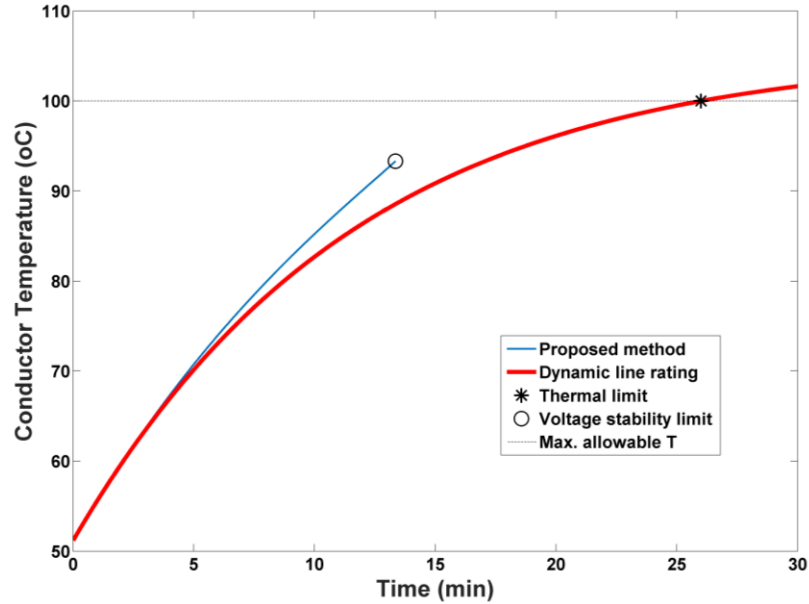


Figure 6.10: Line 1 conductor temperature – Case C

In response to a line 2 outage, line 1 line current increases to 1047 A. Figure 6.9 and Figure 6.10 show how line 1 current and conductor temperature vary with time following the contingency. Using the DLR approach, line 1 reaches  $T_c^{max}$  after 26 minutes. However, the results of the proposed approach indicate that the system is expected to experience voltage stability issues after 13.5 minutes. These results are summarized in Table 6.7. The comparison in branch 1 real power losses between the proposed approach and DLR is presented in Figure 6.11.

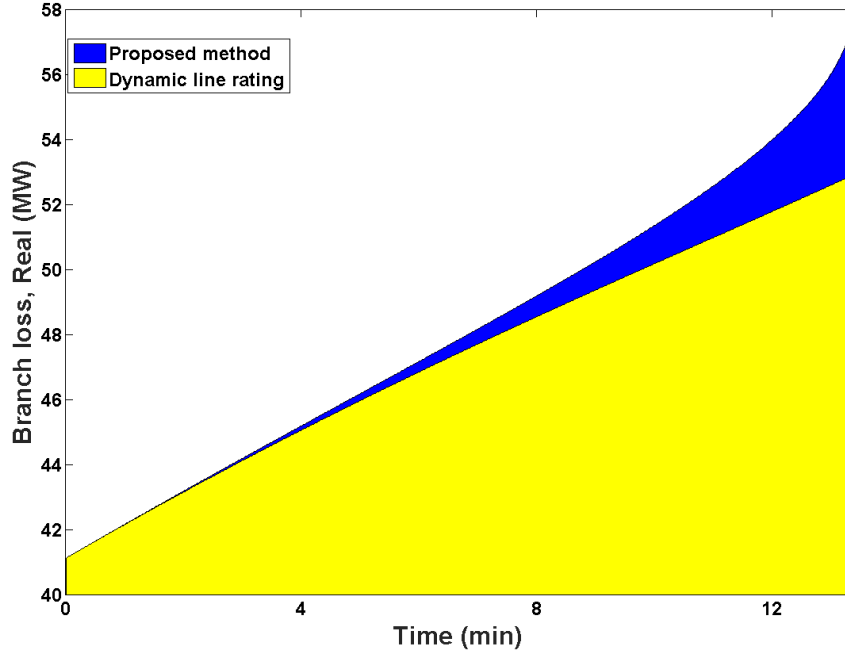


Figure 6.11: Branch 1 conductor temperature – Case C

Table 6.7: Resulting limiting factor and critical time – Case C

	Conventional Method	Proposed Method
Final condition	Thermal limit	Voltage stability limit
Time, $t^{cr}$	26 min	13.5 min

#### 6.4.2 14-Bus System

The proposed temperature-dependent contingency analysis approach is also tested on a 14-bus 20-line test system. The lines under the yellow-shaded region of Figure 6.12 are considered to have available weather measurements from either nearby weather stations or on-line sensors. The measured ambient temperatures and wind speeds associated to each of these lines are shown in Table VII. The rest of the lines are modeled following “static line rating” where pre-defined weather conditions (40°C and 0.5 m/sec) are assumed.

The time required to reach the limiting factor or the new steady-state condition for each line 1-8 contingency, obtained from the proposed method and DLR, are shown in Table 6.8. It can be seen that:

- For line 3 contingency and for line 7 contingency, the system reaches a new steady-state without violating limits;
- For single-line contingencies of lines 4, 5, or 8, at least one line in the system reaches its thermal limit using both approaches, though the time to reach  $T_c^{max}$  is always smaller when computed using the proposed approach than when using DLR;
- For line 6 contingency, one line is expected to reach  $T_c^{max}$  after 30 minutes using the proposed approach, however, according to DLR results the system would reach the new steady-state without violating limits.

Table 6.8: Comparison of time required to reach limiting factor or new steady-state condition

Line Outage	Proposed Approach	Conventional Approach	% diff. in $t^{ci}$
3	New steady state condition	New steady-state condition	-
4	Thermal Limit (Line 2: 11.8 min)	Thermal Limit (Line 2: 13.4 min)	8.5 %
5	Thermal Limit (Line 2: 11.4 min)	Thermal Limit (Line 2: 12.2 min)	6.6 %
6	Thermal Limit (Line 2: 30.8 min)	New steady-state condition	-
7	New steady state condition	New steady-state condition	-
8	Thermal Limit (Line 10: 16.4 min)	Thermal Limit (Line 10: 17.4 min)	5.8%

The observations from the case studies can be summarized as follows:

- The proposed temperature-dependent contingency analysis suggests that a line takes a shorter time to reach its thermal limit following a contingency compared to the DLR approach.
- The proposed approach is capable of determining if the system is approaching a voltage collapse point whereas regular DLR does not provide system voltage conditions.

The proposed approach is capable of incorporating weather conditions and conductor temperatures into steady-state analysis of the power system. It is capable of providing a more realistic representation of the thermal and electrical conditions of the system, and can be beneficial for secure operation and maintenance of power systems.

## CHAPTER 7: CONCLUSION AND FUTURE WORK

### 7.1 Overview

This work presented the coupling of line electrical parameters and weather parameters in order to make a more realistic representation of power systems. The temperature-dependent nature of the line electrical parameters are taken into account for steady-state power flow analysis, as well as for the determination of the power handling capabilities of a system. A temperature dependent power flow method has been developed for that purpose which is capable of –

- Integrating the weather-dependent nature of the line electrical parameters into power flow analysis; and
- Incorporating the longitudinal variation of conductor temperatures and resultant non-uniformity of line parameters into power flow analysis.

Utilizing the outcomes from the proposed power flow method a novel temperature-dependent continuation power flow method is also introduced which helps to determine a more accurate estimation of the system power handling capability considering both thermal and voltage stability limits, compared to the conventional methods. A new parameter named as ‘effective maximum loading parameter’ is introduced in this integrated method which provides information about the maximum loadability of a system.

Uncertainty of the weather conditions are taken into account for the steady-state analysis using an affine arithmetic based power flow method. This approach is capable of

dealing with the uncertainties in any external datasets for power flow analysis. The impact of these uncertainties on the transfer capability of a system is also studied using the proposed affine arithmetic based toolbox.

Impact of the transient thermal conditions of overhead transmission line on the power handling capability of a system is investigated. The temperature-dependent power flow method is utilized in order to track the variation in thermal and voltage stability limits of the system under the non-steady-state heat balance conditions.

The specific contributions of this research work is summarized in the following Section 8.2, and Section 8.3 discusses the future vision of this work.

## 7.2 Summary of Contributions

The contributions of this thesis are as follows:

- Revisiting the formulations of the temperature-dependent line modeling by incorporating the heat balance equation into the line modeling approaches.
  
- Development of a temperature-dependent power flow algorithm using the non-linearized equations of heat gain and heat losses from IEEE Std. 738. The heat balance equation is incorporated into the Newton-Raphson power flow algorithm in such a way that it can provide
  - A more realistic representation of a power system network;
  - Thermal conditions of system branches alongside the electrical parameters;

- Integration of the longitudinal variation of the conductor temperatures into power flow analysis; and
  - The option to integrate data uncertainties in weather and loading conditions into power system analysis.
- Development of a MATLAB-based automated temperature-dependent power flow toolbox.
- Utilization of the proposed temperature-dependent power flow in order to determine the power handling capability of a power system network, in terms of both thermal limit and voltage stability limit. The conventional continuation power flow method is modified thus it can incorporate the variation of line electrical parameters to determine the voltage collapse point as well as the conductor temperature at each step increase in loading parameter. This integrated approach makes it possible to:
  - Determine the thermal and voltage stability limit using a single unified methodology;
  - Obtain a more accurate estimation of the system power transfer limits compared to conventional methods.
  - Consider the impact of variation in weather conditions along the length of transmission lines.
- Development of a temperature-dependent continuation power flow toolbox in MATLAB.
- Introduction of a time-dependent temperature-dependent power system analysis toolbox to account for the transient thermal conditions of

transmission lines. This proposed approach is capable of tracking the change in system thermal and electrical conditions after a change in system load or weather conditions, and provides the system maximum power transfer capability under these non-static thermal conditions. This proposed method can be used to:

- Overcome the limitation of conventional methods which only considers the thermal limit under non-static heat balance but not the change in voltage stability;
  - Determine the critical time for a system to reach its voltage collapse point; and
  - Determine the critical time for a branch in a system to reach its thermal limit; and
- Implementation of affine arithmetic into temperature-dependent power flow and continuation power flow analysis to deal with data uncertainty in weather conditions. This modified version of interval arithmetic based power flow analysis tool enables to get a non-deterministic result of the system power handling capability instead of a single-point fixed value number, assisting a flexible operation of the power system.

### 7.3 Future Work

Several suggestion and considerations can be made based on the completed work in this thesis:

- This work studied the impact of non-static thermal conditions on the thermal and voltage stability limits of a power system, and the critical time to reach the limiting factor. However, outage of a branch in a system or a change in system load will also impact the ranking of the branches which can be determined by a contingency analysis. Therefore, a temperature-dependent contingency ranking analysis could be a possible future work under this project.
- A novel method to incorporate the non-linearized heat balance equation into Newton-Raphson power flow algorithm is presented in this work. Apart from the power flow algorithm, state estimation is another method for steady-state analysis of power system. An updated methodology of integrating the weather conditions and resultant conductor temperatures into state-estimation analysis could be developed without using the linearization of the heat gain and heat loss equations.
- Line model segmentation approach is used in this thesis for the system-level analysis of the longitudinal variation of weather conditions. [47]-[48] showed that the non-uniformly distributed differential approach may have potential to accommodate the longitudinal conductor temperature variation more accurately compared to the line model segmentation, but due to computational complexities the differential approach is not used for system-

level studies in this work. Therefore, studying the impact of spatial variation in weather parameters using the differential approach could be a future study worth consideration.

- A hardware-software based testbed could be setup for experimental evaluation of the proposed line model approaches. Controlled weather chambers can be used along the line in the testbed to create longitudinal variation in conductor temperatures. The testbed could also be used to determine the behavior of the rise in conductor temperature during a change in electrical loading conditions. The experimental results for the increase in conductor temperature for a step increase in system load can be compared with the proposed approach in this thesis, and with the conventional approach.
- This thesis investigated the impact of variation in weather conditions and line currents on transmission networks consisting of overhead AC transmission lines, as till now most of the transmission lines are AC and overhead. However, the variation in external conditions and line currents can also impact the HVDC transmission lines, as well as the underground lines. The impact of longitudinal variation in conductor temperature on these types of transmission lines is another possible research work worth investigating.

## REFERENCES

- [1] S. D. Foss and R. A. Maraio, "Dynamic line rating in the operating environment," in *IEEE Transactions on Power Delivery*, vol. 5, no. 2, pp. 1095-1105, April 1990.
- [2] S. Karimi, P. Musilek and A.M. Knight, "Dynamic thermal rating of transmission lines: A review," in *Renewable and Sustainable Energy Reviews*, vol. 91, pp. 600-612, August 2018.
- [3] B. S. Howington and G. J. Ramon, "Dynamic Thermal Line Rating Summary and Status of the State-of-the-Art Technology," in *IEEE Transactions on Power Delivery*, vol. 2, no. 3, pp. 851-858, July 1987.
- [4] V. Cecchi, A. S. Leger, K. Miu and C. O. Nwankpa, "Modeling Approach for Transmission Lines in the Presence of Non-Fundamental Frequencies," in *IEEE Transactions on Power Delivery*, vol. 24, no. 4, pp. 2328-2335, Oct. 2009.
- [5] J.A.B. Faria, "Nonuniform transmission-line structures: internal and external propagation parameters," in *Electrical Engineering*, vol. 87. Issue 1, pp. 19-22, January 2005.
- [6] A. Benato, R. Paolucci, R. Turri, "Insulated Ground Wire Capacitive Currents for Tower Discharge Warning Lamp Supplying," *Electric Power Systems Research*, Vol. 71/3, pp. 211-221, November 2004.
- [7] M. D. Ilic, Y. Makarov and D. Hawkins, "Operations of Electric Power Systems with High Penetration of Wind Power: Risks and Possible Solutions," 2007 IEEE Power Engineering Society General Meeting, Tampa, FL, 2007, pp. 1-4.
- [8] *Renewable Energy Sources and Climate Change Mitigation U.K.* Cambridge: Cambridge Univ. Press 2012.
- [9] E. Denny and M. O'Malley, "Wind generation, power system operation, and emissions reduction," in *IEEE Transactions on Power Systems*, vol. 21, no. 1, pp. 341-347, Feb. 2006.

- [10] R. D. Christie, B. F. Wollenberg and I. Wangensteen, "Transmission management in the deregulated environment," in Proceedings of the IEEE, vol. 88, no. 2, pp. 170-195, Feb. 2000.
- [11] G. Cliteur, A. vanderWal and D. Novosel, "Improving Transmission Performance without Replacing Equipment", Utility Automation, Page(s): 28-32, March/April 2004.
- [12] H.E. House, P.D. Tuttle, "Current carrying capacity of ACSR", AIEE Transaction on Power Apparatus and Systems, Part III, vol. 77, issue 3, February 1959, pp. 1169-1177.
- [13] K.E. Holbert, G.T. Heydt, "Prospects for dynamic transmission circuit ratings", The 2001 IEEE International Symposium on Circuits and Systems, 2001. ISCAS 2001. Vol. 3, pp. 205-208, 6-9 May 2001.
- [14] IEEE Standard for Calculating the Current-Temperature Relationship of Bare Overhead Conductors," in IEEE Std 738-2012 (Revision of IEEE Std 738-2006 - Incorporates IEEE Std 738-2012 Cor 1-2013), vol., no., pp.1-72, Dec. 23 2013.
- [15] CIGRE Working Group Study Committee 22 Working Group 12, "Thermal Behaviour of Overhead Conductors", CIGRE Technical Brochure 207, August 2002.
- [16] C. R. Black and W. A. Chisholm, "Key Considerations for the Selection of Dynamic Thermal Line Rating Systems," in IEEE Transactions on Power Delivery, vol. 30, no. 5, pp. 2154-2162, Oct. 2015.
- [17] S. D. Foss, S. H. Lin, H. R. Stillwell and R. A. Fernandes, "Dynamic Thermal Line Ratings Part II Conductor Temperature Sensor and Laboratory Field test Evaluation," in IEEE Transactions on Power Apparatus and Systems, vol. PAS-102, no. 6, pp. 1865-1876, June 1983.
- [18] E. E. Hutchings, R. G. Parr, Current-Carrying Capacity of Bare Stranded Conductors, 1949.
- [19] H. Wan, J. D. McCalley and V. Vittal, "Increasing thermal rating by risk analysis," in IEEE Transactions on Power Systems, vol. 14, no. 3, pp. 815-828, Aug. 1999.
- [20] Y. Wu, S. Lou and S. Lu, "A Model for Power System Interconnection Planning Under Low-Carbon Economy With CO<sub>2</sub> Emission Constraints,"

- in IEEE Transactions on Sustainable Energy, vol. 2, no. 3, pp. 205-214, July 2011.
- [21] C. R. Black and W. A. Chisholm, "Key Considerations for the Selection of Dynamic Thermal Line Rating Systems," in IEEE Transactions on Power Delivery, vol. 30, no. 5, pp. 2154-2162, Oct. 2015.
- [22] R. Stephen, "Description and evaluation of options relating to uprating of overhead transmission lines." CIGRÉ Session, V2-201, Paris (2004).
- [23] Michiorri, A., Taylor, P.C., Jupe, S.C.E., and Berry, C.J., "Investigation into the influence of environmental conditions on power system ratings", Proceedings of the Institution of Mechanical Engineers, Vol. 223, Part A: Journal of Power and Energy, 2009.
- [24] S. N. K. M. Jagarlapudi and V. Cecchi, "Investigating wind speed-dependent models for electric power transmission lines," 2016 IEEE International Symposium on Circuits and Systems (ISCAS), Montreal, QC, 2016, pp. 626-629.
- [25] M. Rahman, M. Kiesau, V. Cecchi and B. Watkins, "Investigating the impacts of conductor temperature on power handling capabilities of transmission lines using a multi-segment line model," SoutheastCon 2017, Charlotte, NC, 2017, pp. 1-7.
- [26] W. F. Tinney and C. E. Hart, "Power Flow Solution by Newton's Method," in IEEE Transactions on Power Apparatus and Systems, vol. PAS-86, no. 11, pp. 1449-1460, Nov. 1967.
- [27] J. Grainger, W.D. Stevenson, "Power System Analysis," New York, Macgraw-Hill, 1994, ch. 6, pp. 193-230.
- [28] A. K. Laha, K. E. Bollinger, R. Billinton and S. B. Dhar, "Modified form of Newton's method for faster load-flow solutions," in Proceedings of the Institution of Electrical Engineers, vol. 121, no. 8, pp. 849-853, August 1974.
- [29] Aluminum Electrical Conductor Handbook, 3rd edition, The Aluminum Association, 1989.

- [30] M. Bockarjova and G. Andersson, "Transmission Line Conductor Temperature Impact on State Estimation Accuracy," 2007 IEEE Lausanne Power Tech, Lausanne, 2007, pp. 701-706.
- [31] Frank, S., Sexauer, J., Mohagheghi, S.: 'Temperature-dependent power flow', IEEE Transaction on Power Systems., 2013, 28, (4), pp. 4007–4018
- [32] IEEE Standard for Calculating the Current-Temperature Relationship of Bare Overhead Conductors," in IEEE Std 738-2012 (Revision of IEEE Std 738-2006 - Incorporates IEEE Std 738-2012 Cor 1-2013), vol., no., pp.1-72, Dec. 23 2013.
- [33] M. M. Esfahani and G. R. Yousefi, "Real Time Congestion Management in Power Systems Considering Quasi-Dynamic Thermal Rating and Congestion Clearing Time," in IEEE Transactions on Industrial Informatics, vol. 12, no. 2, pp. 745-754, April 2016.
- [34] F. Capitanescu, T. Van Cutsem, "A unified management of congestions due to voltage instability and thermal overload," in Electric Power Systems Research, vol. 77, issue 10, pp. 1274-1283, 2007.
- [35] X. Dong et al., "Calculation of Power Transfer Limit Considering Electro-Thermal Coupling of Overhead Transmission Line," in IEEE Transactions on Power Systems, vol. 29, no. 4, pp. 1503-1511, July 2014.
- [36] R. Adapa and D. A. Douglass, "Dynamic thermal ratings: monitors and calculation methods," 2005 IEEE Power Engineering Society Inaugural Conference and Exposition in Africa, Durban, 2005, pp. 163-167.
- [37] J. S. Engelhardt and S. P. Basu, "Design, installation, and field experience with an overhead transmission dynamic line rating system," Proceedings of 1996 Transmission and Distribution Conference and Exposition, Los Angeles, CA, USA, 1996, pp. 366-370.
- [38] B. Xu, A. Ulbig and G. Andersson, "Impacts of dynamic line rating on power dispatch performance and grid integration of renewable energy sources," IEEE PES ISGT Europe 2013, Lyngby, 2013, pp. 1-5.
- [39] H.W. Beaty, "Handbook of Electric Power Calculations", 3rd ed., New York: McGraw-Hill, 2001.

- [40] Aluminum Electrical Conductor Handbook, 3rd edition, The Aluminum Association, 1989.
- [41] V. Cecchi, A. S. Leger, K. Miu and C. O. Nwankpa, "Incorporating Temperature Variations Into Transmission-Line Models," in IEEE Transactions on Power Delivery, vol. 26, no. 4, pp. 2189-2196, Oct. 2011.
- [42] A.S. AlFuhaid, E.A. Oufi, and M.M. Saied, "Application of nonuniform-line theory to the simulation of electromagnetic transients in power systems," in International Journal of Electrical Power & Energy Systems, vol. 20, issue 3, pp. 225-233, March 1998.
- [43] A. T. Starr, "The Nonuniform Transmission Line," in Proceedings of the Institute of Radio Engineers, vol. 20, no. 6, pp. 1052-1063, June 1932.
- [44] G. Miano, A. Maffucci, "Transmission Lines and Lumped Circuits: Fundamentals and Applications," San Diego, USA, Academic Press, 2001.
- [45] H. V. Nguyen, H. W. Dommel and J. R. Marti, "Modelling of single-phase nonuniform transmission lines in electromagnetic transient simulations," in IEEE Transactions on Power Delivery, vol. 12, no. 2, pp. 916-921, April 1997.
- [46] Yaqing Liu, N. Theethayi and R. Thottappillil, "An engineering model for transient analysis of grounding system under lightning strikes: nonuniform transmission-line approach," in IEEE Transactions on Power Delivery, vol. 20, no. 2, pp. 722-730, April 2005.
- [47] V. Cecchi, M. Knudson, K. Miu and C. Nwankpa, "A non-uniformly distributed parameter transmission line model," 2012 North American Power Symposium (NAPS), Champaign, IL, 2012, pp. 1-6.
- [48] C. Braun, M. Rahman and V. Cecchi, "A transmission line model with non-uniformly distributed line impedance," 2017 North American Power Symposium (NAPS), Morgantown, WV, 2017.
- [49] V. Cecchi, M. Knudson and K. Miu, "System Impacts of Temperature-Dependent Transmission Line Models," in IEEE Transactions on Power Delivery, vol. 28, no. 4, pp. 2300-2308, Oct. 2013.

- [50] C. S. Cheng and D. Shirmohammadi, "A three-phase power flow method for real-time distribution system analysis," in *IEEE Transactions on Power Systems*, vol. 10, no. 2, pp. 671-679, May 1995.
- [51] P. Zarco and A. G. Exposito, "Power system parameter estimation: a survey," in *IEEE Transactions on Power Systems*, vol. 15, no. 1, pp. 216-222, Feb. 2000.
- [52] V. Knyazkin, C. A. Canizares and L. H. Soder, "On the parameter estimation and modeling of aggregate power system loads," in *IEEE Transactions on Power Systems*, vol. 19, no. 2, pp. 1023-1031, May 2004.
- [53] F. F. Wu, "Power system state estimation: a survey," in *International Journal of Electrical Power & Energy Systems*, vol. 12, no. 2, pp. 80-87, April 1990.
- [54] M. Rahman, M. Kiesau, V. Cecchi and B. Watkins, "Investigating the impacts of conductor temperature on power handling capabilities of transmission lines using a multi-segment line model," *SoutheastCon 2017*, Charlotte, NC, 2017, pp. 1-7.
- [55] H. Banakar, N. Alguacil and F. D. Galiana, "Electrothermal coordination part I: theory and implementation schemes," in *IEEE Transactions on Power Systems*, vol. 20, no. 2, pp. 798-805, May 2005.
- [56] N. Alguacil, M. H. Banakar and F. D. Galiana, "Electrothermal coordination part II: case studies," in *IEEE Transactions on Power Systems*, vol. 20, no. 4, pp. 1738-1745, Nov. 2005.
- [57] W. Sun, Y. Zhang, C. Wang and P. Song, "Flexible load shedding strategy considering real-time dynamic thermal line rating," in *IET Generation, Transmission & Distribution*, vol. 7, no. 2, pp. 130-137, Feb. 2013.
- [58] H.T. Jadhav, P. D. Bamane. "Temperature dependent optimal power flow using g-best guided artificial bee colony algorithm." *International Journal of Electrical Power & Energy Systems* 77: 77-90, 2016.
- [59] U. Nowak, and L. Weimann, "A family of Newton Codes for systems of highly nonlinear equations," *Konrad-Zuse-Zentrum für Informationstechnik Berlin*, 1991.

- [60] N. Sato and W. F. Tinney, "Techniques for exploiting the sparsity of the network admittance matrix," *IEEE Transactions on Power Apparatus and Systems.*, vol. PAS-82, no. 69, pp. 944–950, Dec. 1963.
- [61] A. M. Kettner and M. Paolone, "On the Properties of the Power Systems Nodal Admittance Matrix," in *IEEE Transactions on Power Systems*, vol. 33, no. 1, pp. 1130-1131, Jan. 2018.
- [62] A. Arguez, I. Durre, S. Applequist, M. Squires, R. Vose, X. Yin and R. Bilotta, NOAA's U.S. Climate Normals (1981-2010). [Air Temperature hourly normal, wind speed average]. NOAA National Centers for Environmental Information, 2010.
- [63] A. Bergen, V. Vittal, J., *Power System Analysis*. New Jersey: Prentice-Hall Inc, 2000.
- [64] V. Ajjarapu and C. Christy, "The continuation power flow: a tool for steady state voltage stability analysis," in *IEEE Transactions on Power Systems*, vol. 7, no. 1, pp. 416-423, Feb. 1992.
- [65] A. Piccolo, A. Vaccaro and D. Villacci, "An Affine arithmetic based methodology for the thermal rating assessment of overhead lines in the presence of data uncertainty," 2003 IEEE Bologna Power Tech Conference Proceedings,, Bologna, Italy, 2003, pp. 7 pp. Vol.4-.
- [66] A. Vaccaro, C. A. Canizares and D. Villacci, "An Affine Arithmetic-Based Methodology for Reliable Power Flow Analysis in the Presence of Data Uncertainty," in *IEEE Transactions on Power Systems*, vol. 25, no. 2, pp. 624-632, May 2010.
- [67] Gu, W.; Luo, L.; Ding, T.; Meng, X.; Sheng, W. An affine arithmetic-based algorithm for radial distribution system power flow with uncertainties. *Int. J. Electr. Power Energy Syst.* 2014, 58, 242–245.
- [68] M. Rahman, M. Kiesau, V. Cecchi and B. Watkins, "Investigating effects of weather parameter uncertainty on transmission line power handling capabilities using affine arithmetic," 2017 IEEE Power & Energy Society General Meeting, Chicago, IL, 2017, pp. 1-5.
- [69] C. Rakpenthai, S. Uatrongjit and S. Premrudeepreechacharn, "State estimation of power system considering network parameter uncertainty based on

- parametric interval linear systems," PES T&D 2012, Orlando, FL, 2012, pp. 1-1.
- [70] L.E.S. Pereira, V.M. da Costa, "Interval analysis applied to the maximum loading point of electric power systems considering load data uncertainties," *International Journal of Electrical Power & Energy Systems*, vol. 54, pp. 334-340, January 2014.
- [71] B. Das, "Radial distribution system power flow using interval arithmetic," *International Journal of Electrical Power & Energy Systems*, vol. 24, Issue 10, pp. 827-836, December 2002.
- [72] L.H. De Figueiredo L. Henrique J. Stolfi "Affine arithmetic: concepts and applications" *Numerical Algorithms* vol. 37.1-4 pp. 147-158 2004.
- [73] T. Hickey, Q. Ju and M.H. Van Emden, "Interval arithmetic: From principles to implementation," *Journal of the ACM (JACM)* 48.5 (2001): 1038-1068.
- [74] D. Degrauwe G. Lombaert G. De Roeck "Improving interval analysis in finite element calculations by means of affine arithmetic" *Computers & structures* vol. 88.3 pp. 247-254 2010.
- [75] J. Stolfi and L.H. De Figueiredo. "An introduction to affine arithmetic." *Trends in Applied and Computational Mathematics* 4.3 (2003): 297-312.
- [76] H. Shaalan, "Transmission line analysis using interval mathematics," 2012 North American Power Symposium (NAPS), Champaign, IL, 2012, pp. 1-5.
- [77] P.Umapathy, C. Venkatasessaiah, and M. Senthil Arumugam, "Application of Interval Arithmetic in the Evaluation of Transfer Capabilities by Considering the Sources of Uncertainty," *Discrete Dynamics in Nature and Society*, vol. 2009, Article ID 527385, 12 pages, 2009.
- [78] J. Heckenbergerova, P. Musilek and K. Filimonenkov, "Assessment of seasonal static thermal ratings of overhead transmission conductors," 2011 IEEE Power and Energy Society General Meeting, Detroit, MI, USA, 2011, pp. 1-8.
- [79] S. S. Kaddah, K. M. Abo-Al-Ez, T. F. Megahed and M. G. Osman, "Probabilistic unit commitment in multi-area grids with high renewable energy penetration by using dynamic programming based on Neural

- Network," International Conference on Renewable Power Generation (RPG 2015), Beijing, 2015, pp. 1-6.
- [80] M. Mahmoudian Esfahani and G. R. Yousefi, "Real Time Congestion Management in Power Systems Considering Quasi-Dynamic Thermal Rating and Congestion Clearing Time," in *IEEE Transactions on Industrial Informatics*, vol. 12, no. 2, pp. 745-754, April 2016.
- [81] M. Rahman, F. Atchison and V. Cecchi, "Grid Integration of Renewable Energy Sources: Utilization of Line Thermal Behavior," *SoutheastCon 2019*, Huntsville, AL, 2019, pp. 1-6.
- [82] M. Rahman, C. Braun, V. Cecchi and B. Watkins, "Study of the Impact of Load Step Changes on Thermal and Voltage Stability Limits of Overhead Transmission Lines," *SoutheastCon 2018*, St. Petersburg, FL, 2018.
- [83] I. A. Hiskens and M. A. Pai, "Hybrid systems view of power system modelling," 2000 IEEE International Symposium on Circuits and Systems. Emerging Technologies for the 21st Century. Proceedings (IEEE Cat No.00CH36353), Geneva, Switzerland, 2000, pp. 228-231 vol.2.
- [84] I. A. Hiskens and M. A. Pai, "Trajectory sensitivity analysis of hybrid systems," in *IEEE Transactions on Circuits and Systems I: Fundamental Theory and Applications*, vol. 47, no. 2, pp. 204-220, Feb. 2000.
- [85] G. K. Morison, B. Gao and P. Kundur, "Voltage stability analysis using static and dynamic approaches," in *IEEE Transactions on Power Systems*, vol. 8, no. 3, pp. 1159-1171, Aug. 1993.
- [86] M. K. Donnelly, J. E. Dagle, D. J. Trudnowski and G. J. Rogers, "Impacts of the distributed utility on transmission system stability," in *IEEE Transactions on Power Systems*, vol. 11, no. 2, pp. 741-746, May 1996.
- [87] K. Cheung, H. Wu, "Implementation of Dynamic Thermal Ratings in the Operational Environment", *FERC Technical Conference: Increasing Real-Time and Day-Ahead Market Efficiency through Improved Software*, June, 2014.
- [88] R. D. Zimmerman, C. E. Murillo-Sánchez, and R. J. Thomas, "MATPOWER: Steady-State Operations, Planning and Analysis Tools for Power Systems

Research and Education," Power Systems, IEEE Transactions on, vol. 26, no. 1, pp. 12-19, Feb. 2011.

## APPENDICES

APPENDIX A: LINE MODEL SEGMENTATION

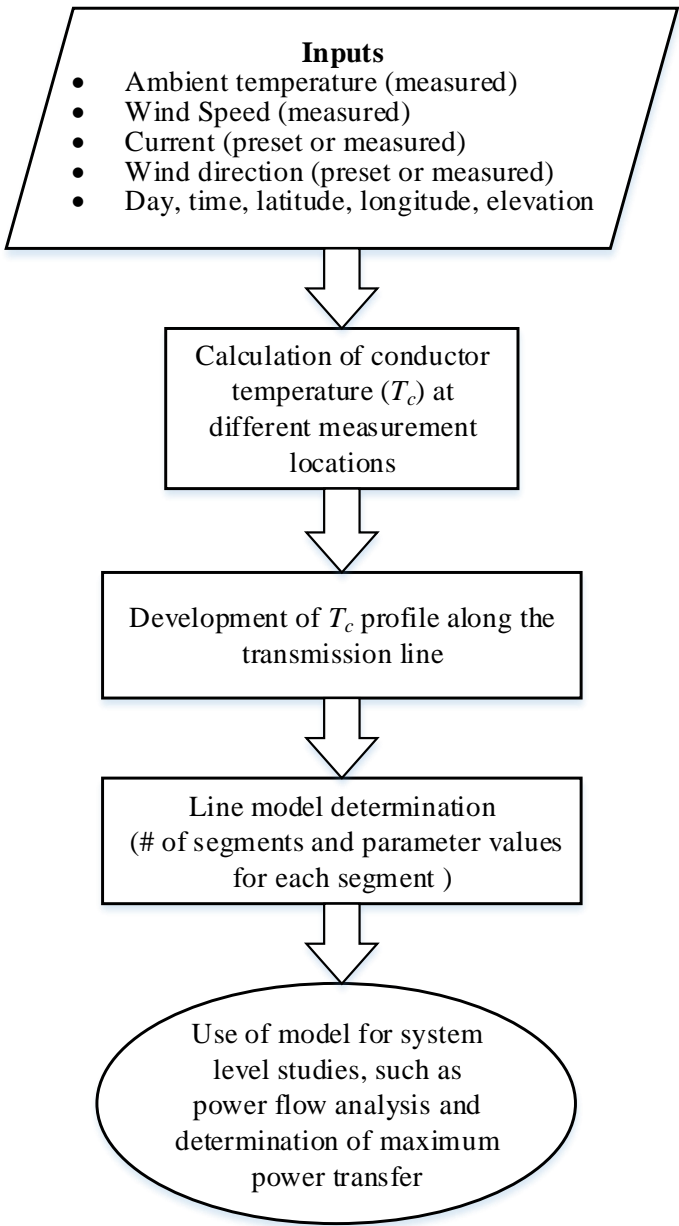


Figure A1: Process for multi-segment line modeling

Line Model Segmentation: Examples

Table A1: Weather conditions for example cases

Case	Location	1	2	3	4	5
I	Wind Speed (m/s)	1	1.1	0.9	1.1	1.2
	Ambient Temp ( <sup>0</sup> C)	35	33	31	36	33
II	Wind Speed (m/s)	0.9	1.15	1.5	1.8	2.25
	Ambient Temp ( <sup>0</sup> C)	33	31	28	26	25
III	Wind Speed (m/s)	1	1.7	2.5	3.2	4.5
	Ambient Temp ( <sup>0</sup> C)	35	30	26	20	15

Case I: Minor Change in Weather Conditions

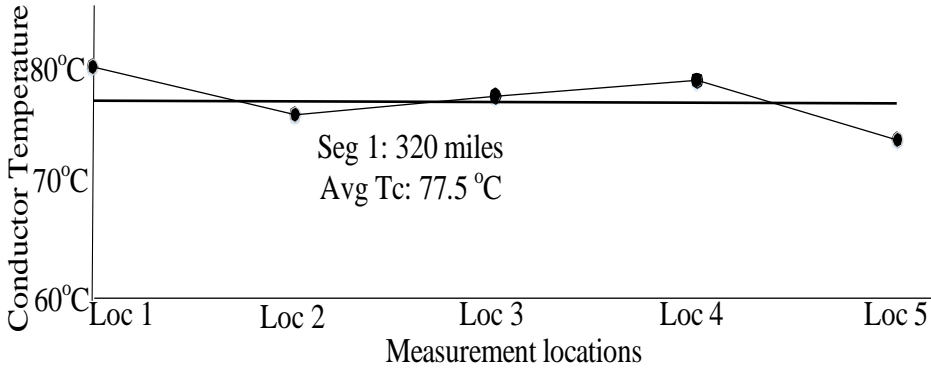


Figure A2:  $T_c$  profile for case I

Table A2: Output from line model segmentation - case I

# of segments	Segment number	Segment length (mi)	Conductor Temp. $T_c$ ( $^{\circ}\text{C}$ )	Resistance $R_{TC}$ (ohm/mi)
1	Seg 1	320	77.5	0.1733

Case II: Gradual Change in Weather Conditions

Table A3: Output from line model segmentation - case II

# of segments	Segment number	Segment length (mi)	$T_c$	Resistance $R_{TC}$ (ohm/mi)
2	Seg 1	160	72.65	0.1710
	Seg 2	160	60	0.1650

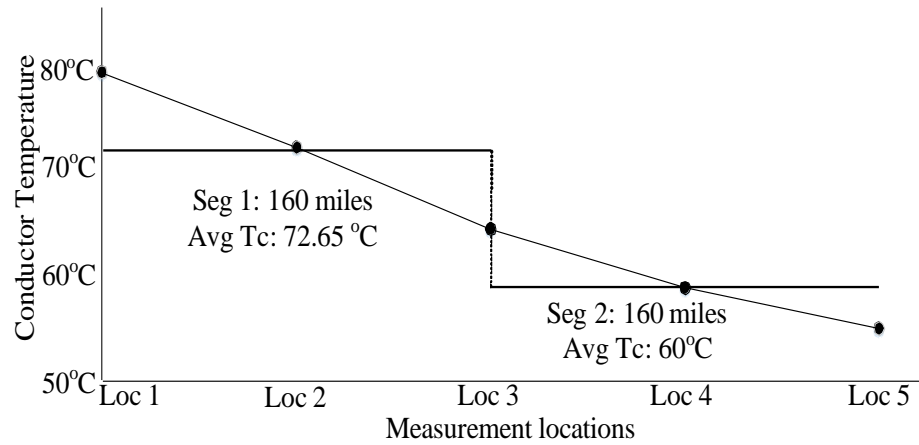
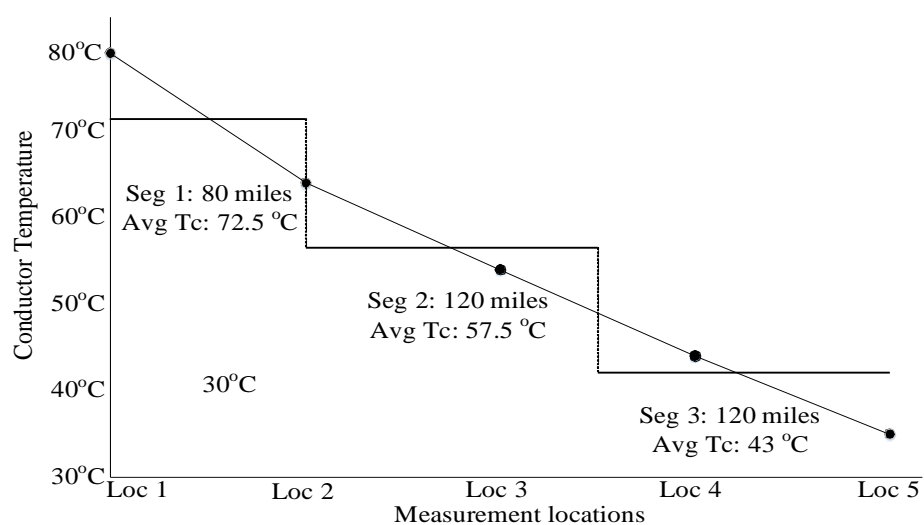


Figure A3:  $T_c$  profile for case II

## Case III: Steep Change in Weather Conditions

Table A3: Output from line model segmentation - case III

# of segments	Segment number	Segment length (mi)	$T_c$	Resistance $R_{TC}$ (ohm/mi)
3	Seg 1	80	72.5	0.1709
	Seg 2	120	57.5	0.1639
	Seg 3	120	43	0.1570

Figure A3:  $T_c$  profile for case III

## APPENDIX B: GENERIC CODES

## B.1 Conductor temperature from Heat Balance Equation

```

function Tc = HBEss(I)
Ta = 35;
He = 00;
k_ang = 1;
V_wind = 1; %meter/sec
-----ACSR parameters -----
%R_high = 8.688e-5; R_high = 9.9565e-05;
%R_low = 7.283e-5;
R_low = 9.0745e-05;
%T_high = 75;
T_high = 50;
%T_low = 25;
T_low = 20;
D0 = .0248158;
-----Solar heat gain (calculated seperately)-----
Qs=22.4;
%%
E = 0.75; % Emissiity
% vec = zeros(1,150);
% I = 600; %Amps; %Current (Steady State)
Ts = 30;
msg = 0;
-----Calculation of Tc -----
while msg ~= 1
    T_film = (Ts + Ta)/2;
    kf = .02424+7.477e-5*T_film-4.407e-9*T_film^2;
    uf = (1.458e-6*(T_film+273)^1.5)/(T_film+383.4);
    pf = (1.293-1.525e-4*He+6.379e-9*He^2)/(1+.00367*T_film);
    N_Re = (D0*pf*V_wind)/uf;
    Qc = k_ang*(1.01+1.35*N_Re^.52)*kf*(Ts-Ta);
    Qr = 17.8*D0*E*((Ts+273)./100).^4 - ((Ta+273)./100)^4);
    % R_Ts = ((R_high - R_low)/(T_high - T_low))* (Ts - T_low) + R_low;
    R_Ts = rt(Ts)/1610;
    I_hbe = sqrt((Qc + Qr -Qs)./R_Ts);
    if I_hbe <= I
        Ts=Ts+.01;
        msg = 2;
    else msg = 1;
    end
end

Tc = Ts;
end

```

## B.2 Temperature-Dependent Power Flow

The following is a generic code and user needs to define parameters according to the system for the study. MATPOWER toolbox [88] also needs to be installed and coupled with the following code.

```

declare line lengths
declare external control parameters
declare initial value of Tc = Tc0

Tc = Tc0

msg = 0;
i = 1;
while (msg~=1) & (max(Tc) <= Tc_max) & (msg~=4) & (msg~=3)

    mpcb = loadcase(loadcase);
    get_branch = size(mpcb.branch); % Number of branches
    num_branch = get_branch(1);

    Zbase = mpcb.bus(1,10)^2/mpcb.baseMVA;

    %% Set Resistance
    for m=1:1:num_branch
        mpcb.branch(m,3) = rt(Tc0(m)).*L(m)/Zbase;
        mpcb.branch(m,4) = 0.75.*L(m)/Zbase;
        mpcb.branch(m,5) = 5.1467e-6*L(m)*Zbase;
    end

    results0 = runpf(mpcb);

    if results0.success == 0
        msg = 4;
    end

    %% Current for Baseload
    for u=1:1:num_branch
        I(u) =
get_current(sqrt(results0.branch(u,14)^2+results0.branch(u,15)^2), results0.bus((results0.branch(u,1)),8), results0.bus((results0.branch(u,1)),10));
    end
    n_update = 0;
    timestep_update = 1;

    stamp = [];
    mahi = zeros(5,1);

```

```

while((max(Tc) <= Tc_max) & (msg~=4))
    for k=1:1:num_branch
        newstamp =
HBE(I(k),Tc(k,end),V_wind(k),timestep_update,n_update);
        mahi(k)= newstamp(2);

        k=k+1;

    end

    stamp    = [stamp mahi];

    Tc = stamp;

    for k=1:1:num_branch
mpcb.branch(k,3) = rt(Tc(k,end)).*L(k)/Zbase;
    end

    results = runpf(mpcb);

    if results.success == 0
        msg = 3;
        break
    end

    if size(stamp,2)>1
        for p=1:1:num_branch
            diff(p) = abs(stamp(1,end-1)-stamp(1,end));
        end

        thres    = find(diff<1e-3);

        if thres~[];
            msg = 1;
            break
        end
    end

    for u=1:1:num_branch
        I(u)=
get_current(sqrt(results.branch(u,14)^2+results.branch(u,15)^2),results
.bus((results.branch(u,1)),8),results.bus((results.branch(u,1)),10));
    end

    n_update = n_update+1;

    msg = 2;

end

end

```

## VITA

FULL NAME: Md Mahbubur Rahman  
 DATE AND PLACE OF BIRTH: 12/02/1986, DINAJPUR, BANGLADESH  
 EDUCATION:

Ph.D. Electrical Engineering	UNC Charlotte, NC, USA	2019
M.S. Electrical Engineering	University of Toledo, OH, USA	2015
B.S. Electrical Engineering	Bangladesh Univ. of Eng. & Tech, Bangladesh	2009

## SELECT PUBLICATIONS

- [J1] M. Rahman, V. Cecchi and K. Miu, "Power Handling Capabilities of Transmission Systems Using a Temperature-Dependent Power Flow" *Electrical Power Systems Research*, vol. 149, 2019, pp. 241-249, 2019.
- [J2] M. Rahman, V. Cecchi and K. Miu, "A Temperature-Dependent Power Flow Approach Incorporating Non-Static Conductor Heat Balance" under review at *IEEE Transactions Power Delivery*, January 2019.
- [C1] M. Rahman, C. Braun and V. Cecchi, "Determination of Transmission Line Power Transfer Capabilities Using Temperature Dependent Continuation Power Flow," *2018 IEEE Power & Energy Society General Meeting*, Portland, OR, USA, 2018.
- [C2] M. Rahman, C. Braun and V. Cecchi, "Study of the impact of longitudinal variations in ambient conditions on transmission line voltage stability margin," *2017 North American Power Symposium (NAPS)*, Morgantown, WV, 2017.
- [C3] C. Braun, M. Rahman and V. Cecchi, "A transmission line model with non-uniformly distributed line impedance," *2017 North American Power Symposium (NAPS)*, Morgantown, WV, 2017.
- [C4] C. Braun, M. Rahman and V. Cecchi, "An evaluation of transmission line models incorporating longitudinal temperature variations," *2018 IEEE International Symposium on Circuits and Systems (ISCAS)*, Florence, 2018.
- [C5] M. Rahman, M. Kiesau, V. Cecchi and B. Watkins, "Investigating effects of weather parameter uncertainty on transmission line power handling capabilities using affine arithmetic," *2017 IEEE Power & Energy Society General Meeting*, Chicago, IL, 2017.
- [C6] M. Rahman, M. Kiesau, V. Cecchi and B. Watkins, "Investigating the impacts of conductor temperature on power handling capabilities of transmission lines using a multi-segment line model," *SoutheastCon 2017*, Charlotte, NC, 2017.
- [C7] M. Rahman, C. Braun, V. Cecchi and B. Watkins, "Study of the Impact of Load Step Changes on Thermal and Voltage Stability Limits of Overhead Transmission Lines," *SoutheastCon 2018*, St. Petersburg, FL, 2018.
- [C8] M. Rahman, V. Cecchi, "Conductor Temperature Estimation under Uncertain External Conditions Using a Temperature-Dependent Power Flow," Accepted to *PowerTech Milano 2019*.

- [C9] M. Rahman, F. Atchison and V. Cecchi, "Grid Integration of Renewable Energy Sources: Utilization of Line Thermal Behavior," SoutheastCon 2019, Huntsville, AL, 2019, pp. 1-6.